The Cuboidal Fe_3S_4 Cluster: Synthesis, Stability, and Geometric and Electronic Structures in a Non-Protein Environment

Jian Zhou,[†] Zhengguo Hu,[‡] Eckard Münck,*[,‡] and R. H. Holm*[,†]

Contribution from the Departments of Chemistry, Harvard University, Cambridge, Massachusetts 02138, and Carnegie-Mellon University, Pittsburgh, Pennsylvania 15213

Received November 10, 1995[⊗]

Abstract: Of the three known low-nuclearity iron−sulfur clusters in metallobiomolecules with the core units Fe_2S_2, Fe_4S_4, and Fe_3S_4, the last has not been obtained in stable form outside a protein environment. We describe a direct route to such clusters in the $[Fe_3S_4]^0$ oxidation state, and demonstrate an effective stereochemical and electronic structural congruence with the native cluster. The synthesis is based on iron-site-differentiated clusters. Reaction of $[Fe_4S_4(LS_3)(SEt)]^{2-}$ with $(Et_3NH)(OTf)$ affords $[Fe_4S_4(LS_3)(OTf)]^{2-}$, whose unique site is activated toward terminal ligand substitution. Treatment with 1 equiv of $(Et_4N)_2(Meida)$ affords $[Fe_4S_4(LS_3)(Meida)]^{3-}$, which is readily converted to $[Fe_3S_4(LS_3)]^{3-}$ with 1−2 equiv of additional reactant. The trinuclear cluster is formed by abstraction of Fe^{2+} from a precursor cubane-type $[Fe_4S_4]^{2+}$ core and complexation as $[Fe(Meida)_2]^{2-}$. An analogous procedure starting with $[Fe_4Se_4(LS_3)(SEt)]^{2-}$ yields $[Fe_3Se_4(LS_3)]^{3-}$. The compound $(Et_4N)_3[Fe_3S_4(LS_3)]\cdot MeCN$ crystallizes in orthorhombic space group $P2_12_12_1$ with no imposed symmetry. An X-ray structure solution demonstrates the presence of the desired cuboidal $[Fe_3(\mu_3\text{-}S)(\mu_2\text{-}S)_3]^0$ core in a complex of absolute configuration Δ. Property comparisons support the cuboidal structure for $[Fe_3Se_4(LS_3)]^{3-}$. A series of reactions in the systems $[Fe_4S_4(SEt)_4]^{2-}/(Et_4N)_2(Meida)$ and $[Fe_3S_4(LS_3)]^{3-}/NaSEt$ in Me_2SO disclose that, while cuboidal $[Fe_3S_4(SEt)_3]^{3-}$ is formed in both systems, it is one of several cluster products and tends to decay with time. $[Fe_3S_4(LS_3)]^{3-}$ is completely stable in anaerobic solutions at ambient temperature. Consequently, the semirigid cavitand ligand LS_3 is conspicuously superior to a simple monodentate thiolate in stabilizing the $[Fe_3S_4]^0$ core. The cuboidal core is metrically very similar in structure to the cubane core of $[Fe_4S_4(LS_3)Cl]^{2-}$ and to protein-bound Fe_3S_4 clusters. Voltammetry of $[Fe_3S_4(LS_3)]^{3-}$ reveals a reversible three-membered electron transfer series which includes the core states $[Fe_3S_4]^{1+,0,1-}$. The electronic structures of $[Fe_3S_4(LS_3)]^{3-}$ and $[Fe_3Se_4(LS_3)]^{3-}$ were investigated by Mössbauer and EPR spectroscopies. These studies reveal that the synthetic clusters, like the protein-bound clusters, have an electronic ground state with cluster spin $S = 2$ that arises from an interplay of Heisenberg and double exchange between the sites of a delocalized $Fe^{2+}Fe^{3+}$ pair and an Fe^{3+} site. The zero-field splittings of the $S = 2$ multiplet and the entire set of ^{57}Fe hyperfine parameters of the synthetic clusters match those of the protein-bound clusters. Evidently, protein structure is not required to sustain the cuboidal geometry nor the spin-quintet ground state and its attendant electron distribution and magnetic interactions. We conclude that the clusters $[Fe_3Q_4(LS_3)]^{3-}$ (Q = S, Se) are accurate structural and electronic analogues of the cuboidal sites in native and selenide-reconstituted proteins. No cluster containing a discrete cuboidal Fe_3S_4 core has previously been isolated in substance.

Introduction[1]

The pervasive occurrence in biology of clusters **1** containing the cubane-type Fe_4S_4 core is widely recognized. It has become increasingly evident within the last decade that the structurally derived clusters **2** having the *cuboidal* Fe_3S_4 core are also extensively distributed. Furthermore, this cluster type is intrinsic to at least some proteins rather than necessarily being an artifact arising from oxidative damage of native clusters **1**. Schematic structures of **1** and **2** are set out in Figure 1. The first 3-Fe clusters were recognized by Münck and co-workers,[2] who found from quantitative EPR and Mössbauer measurements one spin associated with three iron atoms in one molecule of *Av* Fd I and *Dg* Fd II.[2] Accounts of early developments in the area are available.[3] Subsequently, these clusters have been extensively characterized by magnetic and spectroscopic means, and structure **2** established crystallographically for inactive aconitase,[4] *Dg* Fd II,[5] and *Av* Fd I[6] in their oxidized ($[Fe_3S_4]^{1+}$) states. *Av* Fd I is representative of 7-Fe proteins which contain one

[†] Harvard University.

[‡] Carnegie Mellon University.

[⊗] Abstract published in *Advance ACS Abstracts,* February 15, 1996.

(1) Abbreviations: *Ac*, *Azotobacter chroococcum*; *Av*, *Azotobacter vinelandii*; bpy, 2,2′-bipyridyl; *Cv*, *Chromatium vinosum*; *Da*, *Desulfovibrio africanus*; *Dg*, *Desulfovibrio gigas*, Fd, ferredoxin; LS_3, 1,3,5-tris((4,6-dimethyl-3-mercaptophenyl)thio)-2,4,6-tris(*p*-tolylthio)benzene(3−); Meida, *N*-methylimidodiacetate; Me_5dien, 1,1,4,7,7-pentamethyldiethylenetriamine; Me_6tren, tris(2-(dimethylamino)ethyl)amine; NHE, normal hydrogen electrode; OTf, triflate; *Pf*, *Pyrococcus furiosus*; Q, S or Se; SCE, standard calomel electrode; Smes, mesitylthiolate(1−); Stibt, 2,4,6-triisopropylbenzenethiolate(1−); tacn, 1,4,7-triazacyclononane.

(2) (a) Emptage, M. H.; Kent, T. A.; Huynh, B. H.; Rawlings, J.; Orme-Johnson, W. H.; Münck, E. *J. Biol. Chem.* **1980**, *255*, 1793. (b) Huynh, B. H.; Moura, J. J. G.; Moura, I.; Kent, T. A.; LeGall, J.; Xavier, A. V.; Münck, E. *J. Biol. Chem.* **1980**, *255*, 3242.

(3) At this stage (1980−1983), the clusters were usually formulated as Fe_3S_3: (a) Beinert, H.; Thomson, A. J. *Arch. Biochem. Biophys.* **1983**, *222*, 333. (b) Münck, E. In *Iron−Sulfur Proteins*; Spiro, T. G., Ed.; Wiley-Interscience: New York, 1982; Chapter 4.

(4) Robbins, A. H.; Stout, C. D. *Proteins* **1989**, *5*, 289.

(5) (a) Kissinger, C. R.; Adman, E. T.; Sieker, L. C.; Jensen, L. H. *J. Am. Chem. Soc.* **1988**, *110*, 8721. (b) Kissinger, C. R.; Sieker, L. C.; Adman, E. T.; Jensen, L. H. *J. Mol. Biol.* **1991**, *219*, 693.

(6) (a) Stout, C. D. *J. Mol. Biol.* **1989**, *205*, 545. (b) Soman, J.; Iismaa, S.; Stout, C. D. *J. Biol. Chem.* **1991**, *266*, 21558. (c) Stout, C. D. *J. Biol. Chem.* **1993**, *268*, 25920.

0002-7863/96/1518-1966$12.00/0

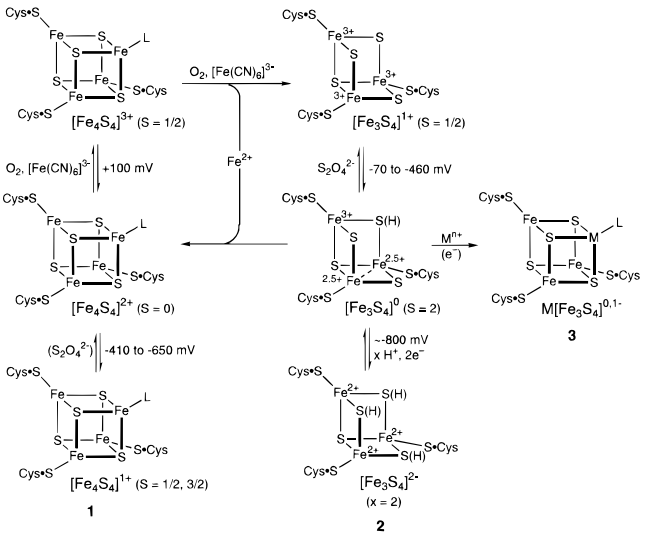

Figure 1. Summary of the oxidation and spin states and the interconversion of Fe_4S_4 and Fe_3S_4 clusters. Terminal ligand L is H_2O/HO^- or a non-cysteinyl protein group. Reported potential limits (vs NHE) for two redox steps are indicated; the single value of the $[Fe_4S_4]^{3+/2+}$ couple is for aconitase.[29] Commonly used redox reagents are shown; dithionite cannot fully reduce $[Fe_4S_4]^{2+/1+}$ couples with the lower potentials. Allowance is made for protonation of $[Fe_3S_4]^{0,2-}$ clusters, but the number of bound protons is uncertain. The all-ferrous $[Fe_3S_4]^{2-}$ core is postulated, not proven.

Fe_3S_4 and one Fe_4S_4 cluster. At least in smaller proteins ($\lesssim$10 kDa), the appearance of an Fe_3S_4 cluster can be correlated with departure from the cysteinyl triplet amino acid sequence Cys-X-X-Cys-X-X-Cys common to the vast majority of proteins which incorporate Fe_4S_4 clusters.[7] In such cases, two Cys residues function as cluster ligands; the remaining Cys ligand of the trinuclear cluster is derived from a residue considerably separated along the chain from the sequence run. For example, in *Da* Fd III,[8] the central Cys residue is replaced by Asp,[9] such that the Fe_3S_4 center is ligated by Cys-11/17/51. When the protein is converted to the 8-Fe form, one Fe_4S_4 cluster retains these three ligands; the remaining Fe site is bound by H_2O/HO^- or possibly the carboxylate group of Asp-14.[10] In the 4-Fe protein *Pf* Fd, the central Cys position is also occupied by Asp, which remains ligated to the cluster in all oxidation states.[11] While this protein does not lose iron during purification, it is readily converted to the Fe_3S_4 form by oxidation.[12]

The study of protein-bound Fe_3S_4 clusters has had a major impact on the magnetochemistry of Fe−S clusters and other exchange-coupled systems. In the reduced state, designated $[Fe_3S_4]^0$, the cluster formally contains two Fe^{3+} and one Fe^{2+}. However, Mössbauer studies of *Av* Fd I and *Dg* Fe II showed that the $S = 2$ cluster ground state consists of a valence-delocalized pair of iron atoms with mean oxidation state $Fe^{2.5+}$ and one valence-trapped Fe^{3+} site.[2] The presence of a delocalized $Fe^{2+}Fe^{3+}$ pair requires a spin coupling model that takes explicitly into account the delocalization. This problem was solved by introduction of a new spin Hamiltonian that includes a resonance delocalization term (double exchange) in addition to the familiar Heisenberg ($JS_i \cdot S_j$) interaction.[13] Inclusion of double exchange led to a picture where the observed $S = 2$ spin of the ground state arises from antiparallel alignment of $S = {}^5/_2$ spin of the Fe^{3+} site with the $S = {}^9/_2$ spin of the delocalized pair; the $S = {}^9/_2$ spin results from parallel alignment of the core spins of the delocalized pair by the itinerant electron.[13] The concept of double exchange, introduced by Zener[14] and further developed by Anderson and Hasegawa,[15] has proven fruitful for the description of the magnetic properties of $[Fe_3S_4]^0$ clusters[13,16−19] and $[Fe_4S_4]^{3+/2+/1+}$ clusters,[16,18−21] as well as the coupled siroheme-Fe_4S_4 chromophore of *E. coli* sulfite reductase.[22] Experimental values of the double exchange parameter, *B*, have not been reported for any Fe−S cluster.[23] However, broken symmetry density functional calculations by Noodleman and co-workers[19] suggest that the double exchange contribution is substantial; namely, $B \approx 700$ cm^{-1} for the $[Fe_4S_4]$ clusters and $B \approx 400$ cm^{-1} for $[Fe_3S_4]^0$ clusters. It has been pointed out[25] that an $S = 2$ ground state could also arise from weak double exchange if different *J* values for the three Fe pairs were considered. On the other hand, Borshch et al.[17] have shown that a combination of *vibronic* interactions and double exchange, even in the absence of Heisenberg−Direc−van Vleck exchange, leads to an $S = 2$ ground state consisting of a delocalized Fe^{2+}-Fe^{3+} pair and a trapped Fe^{3+} site. Most recently, Bominaar et al.[22] have proposed a novel vibronic term that arises from the distance dependence of the double exchange interaction. Clearly, the combination of vibronic interactions with HDvV exchange and double exchange provides a rich new realm of magnetochemical phenomena.

Shortly after the discovery of 3-Fe clusters in *Av* Fd I and *Dg* Fd II, the new cluster type was shown to be present in inactive aconitase. However, when this enzyme was activated by addition of labeled Fe^{2+}, the added ^{57}Fe was found to be incorporated into a subsite of an Fe_4S_4 cluster, demonstrating that the 3-Fe cluster could be converted into the familiar cubane.[26a] This conversion, soon thereafter confirmed and elaborated for *Dg* Fd II,[27] provided a strong hint that the 3-Fe cluster had an Fe_3S_4 core.[3] The observation of reversible $Fe_3S_4 \leftrightarrow Fe_4S_4$ conversions in aconitase and *Dg* Fd II, where three iron sites are protected by the protein matrix, suggested a

(7) Holm, R. H. *Adv. Inorg. Chem.* **1992**, *38*, 1.
(8) (a) Armstrong, F. A.; George, S. J.; Cammack, R.; Hatchikian, E. C.; Thomson, A. J. *Biochem. J.* **1989**, *264*, 265. (b) George, S. J.; Armstrong, F. A.; Hatchikian, E. C.; Thomson, A. J. *Biochem. J.* **1989**, *264*, 275.
(9) Bovier-Lapierre, G.; Bruschi, M.; Bonicel, J.; Hatchikian, E. C. *Biochim. Biophys. Acta* **1987**, *913*, 20.
(10) Butt, J. N.; Sucheta, A.; Armstrong, F. A.; Breton, J.; Thomson, A. J.; Hatchikian, E. C. *J. Am. Chem. Soc.* **1993**, *115*, 1413.
(11) Calzolai, L.; Gorst, C. M.; Zhao, Z.-H.; Teng, Q.; Adams, M. W. W.; La Mar, G. N. *Biochemistry* **1995**, *34*, 11373.
(12) (a) Aono, S.; Bryant, F. O.; Adams, M. W. W. *J. Bacteriol.* **1989**, *171*, 3433. (b) Conover, R. C.; Kowal, A. T.; Fu, W.; Park, J.-B.; Aono, S.; Adams, M. W. W.; Johnson, M. K. *J. Biol. Chem.* **1990**, *265*, 8533.
(13) Papaefthymiou, V.; Girerd, J.-J.; Moura, I.; Moura, J. J. G.; Münck, E. *J. Am. Chem. Soc.* **1987**, *109*, 4703.
(14) Zener, C. *Phys. Rev.* **1951**, *82*, 403.
(15) Anderson, P. W.; Hasegawa, H. *Phys. Rev.* **1955**, *100*, 675.
(16) Sontum, S. F.; Noodleman, L.; Case, D. A. In *The Challenge of d and f Electrons*; Salahub, D. R., Zerner, M., Eds.; ACS Symposium Series 394; American Chemical Society: Washington, DC, 1998; Chapter 26.
(17) Borshch, S. A.; Bominaar, E. L.; Blondin, G.; Girerd, J.-J. *J. Am. Chem. Soc.* **1993**, *115*, 5155.
(18) Bominaar, E. L.; Borshch, S. A.; Girerd, J.-J. *J. Am. Chem. Soc.* **1994**, *116*, 5362.
(19) Noodleman, L.; Case, D. A. *Adv. Inorg. Chem.* **1992**, *38*, 423.
(20) Noodleman, L.; Peng, C. Y.; Case, D. A.; Mouesca, J.-M. *Coord. Chem. Rev.* **1994**, *144*, 199.
(21) Belinskii, M. *Chem. Phys.* **1993**, *173*, 27.
(22) Bominaar, E. L.; Hu, Z.; Münck, E.; Girerd, J.-J.; Borshch, S. *J. Am. Chem. Soc.* **1995**, *117*, 6976.
(23) To date, $[Fe_3S_4]^0$ is the Fe−S cluster with the smallest nuclearity that exhibits valence delocalization. However, an $S = {}^9/_2$ spin state for an $[Fe_2S_2]^{1+}$ cluster has recently been reported.[24] Mössbauer spectroscopy is ideally suited to assess whether the cluster consists of a delocalized Fe^{2+}-Fe^{3+} pair; such studies, however, have not yet been reported.
(24) Crouse, B. R.; Meyer, J.; Johnson, M. K. *J. Am. Chem. Soc.* **1995**, *117*, 9612.
(25) Bertini, I.; Briganti, F.; Luchinat, C. *Inorg. Chim. Acta* **1990**, *175*, 9.
(26) (a) Kent, T. A.; Dreyer, J.-L.; Kennedy, M. C.; Huynh, B. H.; Emptage, M. H.; Beinert, H.; Münck, E. *Proc. Natl. Acad. Sci. U.S.A.* **1982**, *79*, 1096. (b) Emptage, M. H.; Dreyer, J.-L.; Kennedy, M. C.; Beinert, H. *J. Biol. Chem.* **1983**, *258*, 11106. (c) Kent, T. A.; Emptage, M. H.; Merkle, H.; Kennedy, M. C.; Beinert, H.; Münck, E. *J. Biol. Chem.* **1985**, *260*, 6871.

strategy for synthesis of the cubane Fe_3S_4 core that was based on iron-site-differentiated Fe_4S_4 clusters.

Summarized in Figure 1 are the known oxidation and spin ground states of protein-bound Fe_4S_4 and Fe_3S_4 clusters, ranges of redox potentials, and interconversion reactions of clusters and several common reactants which effect them. The upper portion of the scheme, involving the interconversion of clusters **1** and **2**, is drawn largely from the extensive study of aconitase by Beinert, Kennedy, Münck, and their co-workers.[7,26,28] Redox potentials are those of aconitase[29] and, primarily, 7-Fe proteins[8a,30] which exhibit the couples $[Fe_4S_4]^{2+/1+}$ and $[Fe_3S_4]^{1+/0}$; ranges of values are indicated. Chemical oxidation of the $[Fe_4S_4]^{2+}$ state in a variety of proteins yields the $[Fe_3S_4]^{1+}$ ($S = {}^1/_2$) cluster, identified by characteristic MCD and Mössbauer spectra and an EPR signal centered at $g \sim 2.01$. This transformation may proceed by initial formation of the highly oxidized state $[Fe_4S_4]^{3+}$ (normally stable only in the "high-potential" subclass of ferredoxins), an Fe_3S_4 fragment of which is insufficiently electron rich to retain Fe^{2+}. This ion is released and stabilized in solvated or chelated form, affording the oxidized $[Fe_3S_4]^{1+}$ cluster. Indeed, Tong and Feinberg,[29] using direct square-wave voltammetry of aconitase, report detection of the $[Fe_4S_4]^{3+/2+}$ couple at +100 mV and the subsequent spontaneous reaction $[Fe_4S_4]^{3+} \rightarrow [Fe_3S_4]^{1+} + Fe^{2+}$.

With entry to the Fe_3S_4 cluster regime by oxidative cluster degradation, it has been shown that the $[Fe_3S_4]^{1+}$ state of *Da* Fd III has no detectable affinity to bind Fe^{2+} and other divalent ions.[31] Dithionite reduction affords the $[Fe_3S_4]^0$ state. The pH dependence of $[Fe_3S_4]^{1+/0}$ potentials and MCD spectra indicate that one proton is transferred upon reduction in certain cases (aconitase,[29] *Av* Fd I,[30ab] *Ac* Fd I,[30c]) but not another (*Da* Fd III[8a]). All Fe_3S_4 proteins exhibit a second redox process at about −800 mV. In the case of *Da* Fd III, which is the most thoroughly studied,[32] the reduction involves the addition of two electrons and the net uptake of as many as three protons.[33] In Figure 1, we assume for accounting purposes that the reduction product is the all-ferrous $[Fe_3S_4]^{2-}$ cluster, and for it and its precursor we allow for the possibility that the clusters are protonated. Many of the electrochemical features of protein-bound Fe_3S_4 clusters have been summarized by Armstrong.[33]

Whereas analogues of native Fe_2S_2 and Fe_4S_4 clusters are readily prepared,[34,35] extensive attempts in this laboratory to synthesize cuboidal Fe_3S_4 have failed. This core has been prepared, but in its isomeric *linear* $[Fe_3(\mu_2\text{-}S)_4]^{1+}$ configuration.[35] These observations and certain of the results in Figure 1 raise some fundamental questions as to the intrinsic properties of the Fe_3S_4 cluster, among which are the following. (i) Are there synthetic routes to the cluster other than oxidative degradation of an Fe_4S_4 cluster? (ii) Does cuboidal stereochemistry *require* stabilization by a protein matrix or a (thiolate) ligand of special design? (iii) Are the metric features of an Fe_3S_4 cluster closely similar to an Fe_4S_4 "parent" cluster (as protein results indicate[4−6]), or does the cluster relax to significantly different dimensions when, in effect, one iron atom is removed from the parent? (iv) Can the $[Fe_3S_4]^{1-}$ state, as yet undetected in proteins (unless stabilized by binding to a metal cation[30h,31a,36,37]), be attained? And can the all-ferrous $[Fe_3S_4]^{2-}$ state be stabilized with, or without, protonation? (v) Is the potential order $E([Fe_4S_4]^{2+/1+}) \lesssim E([Fe_3S_4]^{1+/0})$ inherent or dependent on protein environment? (vi) Are the fine details of electronic structure (charge distribution, zero-field splitting, ^{57}Fe quadrupole splittings, and hyperfine couplings) dependent on protein structure and its inherent asymmetry? (vii) Will the oxidation states $[Fe_3S_4]^{0,1-}$ bind metal ions and thus offer a general route to heterometal MFe_3S_4 clusters **3** (Figure 1)? No such route to MFe_3S_4 clusters currently exists, these clusters having been prepared by the seemingly disparate methods of self-assembly and reductive rearrangement of linear $[Fe_3S_4]^{1+}$ clusters.[7,38]

Concerning point (i) above, we have recently devised a simple synthetic entry to $[Fe_3S_4]^0$ clusters[39] which we describe in detail here together with structure proof of the cuboidal cluster product. Also, we address points (ii)−(vi), leaving (vii) and the second part of (iv) for subsequent reports. Noting that *apo*-aconitase can be reconstituted to an active ($[Fe_4Se_4]^{2+}$) form with an iron salt and selenide, and converted to an inactive ($[Fe_3Se_4]^{1+}$) form by reaction with ferricyanide,[40] we have included the preparation and characterization of a $[Fe_3Se_4]^0$ cluster in this investigation.

Experimental Section

Preparation of Compounds. All operations were performed under a pure dinitrogen atmosphere using standard glovebox or Schlenk techniques.

$(Bu_4N)_2[Fe_4S_4(LS_3)(CF_3SO_3)]$. To a solution of 214 mg (0.116 mmol) of $(Bu_4N)_2[Fe_4S_4(LS_3)(SEt)]$[41] in 15 mL of acetonitrile was added a solution of 28.7 mg (0.115 mmol) of $(Et_3NH)(CF_3SO_3)$ in 15 mL of acetonitrile. The reaction mixture was stirred for 10 min and filtered. Slow removal of solvent afforded the pure product as a black crystalline solid in quantitative yield. ^1H NMR (CD_3CN): δ 8.24 (5-H), 7.08 (2′-H), 6.81 (3′-H), 5.02 (2-H), 3.93 (4-Me), 3.89 (6-Me), 2.22 (4′-Me).

$(Bu_4N)_2[Fe_4Se_4(LS_3)(SEt)]$. To a solution of 1.00 g (0.788 mmol) of $(Bu_4N)_2[Fe_4Se_4(SEt)_4]$[42] in 150 mL of acetonitrile was added 786

(27) Moura, J. J. G.; Moura, I.; Kent, T. A.; Lipscomb, J. D.; Huynh, B. H.; LeGall, J.; Xavier, A. V.; Münck, E. *J. Biol. Chem.* **1982**, *257*, 6259.
(28) (a) Emptage, M. H. In *Metal Clusters in Proteins*; Que, L., Jr., Ed.; ACS Symposium Series 372; American Chemical Society: Washington, DC, 1988; Chapter 17. (b) Kennedy, M. C.; Stout, C. D. *Adv. Inorg. Chem.* **1992**, *38*, 323.
(29) Tong, J.; Feinberg, B. A. *J. Biol. Chem.* **1994**, *269*, 24920.
(30) (a) Iismaa, S. E.; Vàzquez, A. E.; Jensen, G. M.; Stephens, P. J.; Butt, J. N.; Armstrong, F. A.; Burgess, B. K. *J. Biol. Chem.* **1991**, *266*, 21563. (b) Shen, B.; Martin, L. L.; Butt, J. N.; Armstrong, F. A.; Stout, C. D.; Jensen, G. M.; Stephens, P. J.; La Mar, G. N.; Gorst, C. M.; Burgess, B. K. *J. Biol. Chem.* **1993**, *268*, 25928. (c) Armstrong, F. A.; George, S. J.; Thomson, A. J.; Yates, M. G. *FEBS Lett.* **1988**, *234*, 107. (d) Ohnishi, T.; Blum, H.; Sato, S.; Nakazawa, K.; Hon-nami, K.; Oshima, T. *J. Biol. Chem.* **1980**, *255*, 345. (e) Iwasai, T.; Wakagi, T.; Isogai, Y.; Tanaka, K.; Iizuka, T.; Oshima, T. *J. Biol. Chem.* **1994**, *269*, 29444. (f) Teixeira, M.; Batista, R.; Campos, A. P.; Gomes, C.; Mendes, J.; Pacheco, I.; Anemuller, S.; Hagen, W. R. *Eur. J. Biochem.* **1995**, *227*, 322. (g) Cammack, R.; Rao, K. K.; Hall, D. O.; Moura, J. J. G.; Xavier, A. V.; Bruschi, M.; LeGall, J.; Deville, A.; Gayda, J. P. *Biochim. Biophys. Acta* **1977**, *490*, 311. (h) Moreno, C.; Macedo, A. L.; Moura, I.; LeGall, J.; Moura, J. J. G. *J. Inorg. Biochem.* **1994**, *53*, 219. (i) Battistuzzi, G.; Borsari, M.; Ferretti, S.; Luchinat, C.; Sola, M. *Arch. Biochem. Biophys.* **1995**, *320*, 149.
(31) (a) Butt, J. N.; Armstrong, F. A.; Breton, J.; George, S. J.; Thomson, A. J.; Hatchikian, E. C. *J. Am. Chem. Soc.* **1991**, *113*, 6663. (b) Thomson, A. J.; Breton, J.; Butt, J. N.; Hatchikian, E. C.; Armstrong, F. A. *J. Inorg. Biochem.* **1992**, *47*, 197.
(32) Armstrong, F. A.; Butt, J. N.; George, S. J.; Hatchikian, E. C.; Thomson, A. J. *FEBS Lett.* **1989**, *259*, 15.
(33) Armstrong, F. A. *Adv. Inorg. Chem.* **1992**, *38*, 117.
(34) (a) Berg, J. M.; Holm, R. H. In *Iron−Sulfur Proteins*; Spiro, T. G., Ed.; Wiley: New York, 1982; Chapter 1. (b) Holm, R. H.; Ciurli, S.; Weigel, J. A. *Prog. Inorg. Chem.* **1990**, *29*, 1.
(35) Hagen, K. S.; Watson, A. D.; Holm, R. H. *J. Am. Chem. Soc.* **1983**, *105*, 3905.
(36) Srivastava, K. K. P.; Surerus, K. K.; Conover, R. C.; Johnson, M. K.; Park, J.-B.; Adams, M. W. W.; Münck, E. *Inorg. Chem.* **1993**, *32*, 927.
(37) Finnegan, M. G.; Conover, R. G.; Park, J.-B.; Zhou, Z. H.; Adams, M. W. W.; Johnson, M. K. *Inorg. Chem.* **1995**, *34*, 5358.
(38) (a) Ciurli, S.; Ross, P. K.; Scott, M. J.; Yu, S.-B.; Holm, R. H. *J. Am. Chem. Soc.* **1992**, *115*, 5415. (b) Zhou, J.; Scott, M. J.; Hu, Z.; Peng, G.; Münck, E.; Holm, R. H. *J. Am. Chem. Soc.* **1992**, *114*, 10843.
(39) Zhou, J.; Holm, R. H. *J. Am. Chem. Soc.* **1995**, *117*, 11353.
(40) Surerus, K. K.; Kennedy, M. C.; Beinert, H.; Münck, E. *Proc. Natl. Acad. Sci. U.S.A.* **1989**, *86*, 9846.
(41) (a) Stack, T. D. P.; Holm, R. H. *J. Am. Chem. Soc.* **1988**, *110*, 2484. (b) Liu, H. Y.; Scharbert, B.; Holm, R. H. *J. Am. Chem. Soc.* **1991**, *113*, 9529.
(42) Yu, S.-B.; Papaefthymiou, G. C.; Holm, R. H. *Inorg. Chem.* **1991**, *30*, 3476.

mg (0.828 mmol) of $L(SH)_3$.[43] The reaction mixture was stirred for 12 h, during which it was subjected to dynamic vacuum for 10 min every *ca*. 4 h to remove ethanethiol. The solvent was removed in vacuo; the microcrystalline solid residue was dissolved in 50 mL of acetonitrile and the solution was filtered. Volume reduction of the filtrate caused separation of product as 1.52 g (95%) of black microcrystals. ^{1}H NMR (CD_3CN): δ 15.57 (SCH_2), 8.41 (5-H), 7.02 (2′-H), 6.66 (3′-H), 5.55 (2-H), 4.20 (4-Me), 3.93 (6-Me), 2.21 (4′-Me).

$(Bu_4N)_2[Fe_4Se_4(LS_3)(CF_3SO_3)]$. To a solution of 220 mg (0.108 mmol) of $(Bu_4N)_2[Fe_4Se_4(LS_3)(SEt)]$ in 50 mL of acetonitrile was added a solution of 28.6 mg (0.113 mmol) of $(Et_3NH)(CF_3SO_3)$ in 5 mL of acetonitrile. The reaction mixture was stirred for 10 min and filtered. Slow removal of solvent afforded the pure product as a black crystalline solid in quantitative yield. ^{1}H NMR (CD_3CN): δ 8.51 (5-H), 6.97 (2′-H), 6.62 (3′-H), 5.49 (2-H), 4.38 (4-Me), 4.04 (6-Me), 2.20 (4′-Me).

$(Et_4N)_3[Fe_4S_4(LS_3)(Meida)]$. To a solution of 195 mg (0.101 mmol) of $(Bu_4N)_2[Fe_4S_4(LS_3)(CF_3SO_3)]$ in 10 mL of acetonitrile was added 43 mg (0.106 mmol) of $(Et_4N)_2$(Meida) in 5 mL of acetonitrile. The reaction mixture was stirred for 2 h and filtered. Removal of solvent in vacuo gave a black microcrystalline solid, which was collected and washed with 10 mL of THF and 10 mL of acetone to afford 176 mg (95%) of pure product. Absorption spectrum (Me_2SO): λ_{max} (ϵ_M) 365 (sh, 38 300), 472 (21 200) nm. ^{1}H NMR (Me_2SO): δ 8.55 (5-H), 7.09 (2′-H), 6.58 (3′-H), 4.47 (6-Me), 3.89 (4-Me), 3.49 (CH_2), 3.24 (N-Me), 2.19 (4′-Me), 1.65 (CH_2).

$(Bu_4N)_3[Fe_4S_4(LS_3)(citrate)]$. To a solution of 150 mg (0.078 mmol) of $(Bu_4N)_2[Fe_4S_4(LS_3)(CF_3SO_3)]$ in 5 mL of acetonitrile was added a solution of 45 mg (0.078 mmol) of $(Et_4N)_3$(citrate) in 5 mL of acetonitrile. The mixture was stirred for 1 h, over which time a black microcrystalline solid separated. This material was collected by filtration and washed with THF and acetone, giving 100 mg (65%) of product. ^{1}H NMR (Me_2SO): δ 8.55 (5-H), 7.14 (2′-H), 6.57 (3′-H), 4.47 (6-Me), 3.89 (4-Me), 3.19 (sh, CH_2), 2.14 (4′-Me), 1.37 (CH_2), 0.83 (CH_2).

$(Et_4N)_3[Fe_3S_4(LS_3)]$. To a solution of 210 mg (0.108 mmol) of $(Bu_4N)_2[Fe_4S_4(LS_3)(CF_3SO_3)]$ in 20 mL of acetonitrile was added a solution of 176 mg (0.434 mmol) of $(Et_4N)_2$(Meida) in 5 mL of acetonitrile. The reaction was stirred for 30 min, during which a black microcrystalline solid separated. This material was collected by filtration and washed with 10 mL of THF, 10 mL of acetone, and 5 mL of acetonitrile to yield 140 mg (80%) of pure product. Absorption spectrum (Me_2SO): λ_{max} (ϵ_M) 365 (sh, 28 300), 475 (br sh, 13 100) nm. ^{1}H NMR spectrum (Me_2SO): δ 15.48 (5-H), 11.66 (6-Me), 8.51 (4-Me), 7.06 (2′-H), 6.38 (3′-H), 2.36 (4′-Me). Anal. Calcd for $C_{75}H_{105}Fe_3N_3S_{13}$: C, 55.02; H, 6.46; Fe, 10.23; N, 2.57; S, 25.46. Found: C, 54.86; H, 6.74; Fe, 10.35; N, 2.53; S, 25.38.

$(Et_4N)_3[Fe_3Se_4(LS_3)]$. To a solution of 200 mg (0.094 mmol) of $(Bu_4N)_2[Fe_4Se_4(LS_3)(CF_3SO_3)]$ in 10 mL of acetonitrile was added a solution of 153 mg (0.377 mmol) of $(Et_4N)_2$(Meida) in 5 mL of acetonitrile. The solution was stirred for 10 min, filtered, and allowed to stand overnight. The black crystalline solid was collected by filtration and washed with THF and acetone to give 150 mg (87%) of product. Absorption spectrum (Me_2SO): λ_{max} (ϵ_M) 357 (sh, 77 000), 465 (br sh, 35 200). ^{1}H NMR (Me_2SO, 297 K): δ 15.94 (5-H), 12.12 (6-Me), 9.97 (4-Me), 7.01 (2′-H), 6.25 (3′-H), 2.24 (4′-Me). Anal. Calcd for $C_{75}H_{105}Fe_3N_3S_9Se_4$: C, 49.48; H, 5.81; Fe, 9.20; N, 2.30; S, 15.85; Se, 17.35. Found: C, 49.29; H, 5.99; Fe, 9.15; N, 2.25; S, 16.03; Se, 17.21.

$(Et_4N)_2[Fe(Meida)_2]$. This compound was generated in solution by the reaction of 1 equiv of $Fe(CF_3SO_3)_2$ with 2 or more equiv of $(Et_4N)_2$(Meida); ^{1}H NMR spectra were recorded for purpose of identifying $[Fe(Meida)_2]^{2-}$ formed in the iron abstraction reactions of Figure 2. CD_3CN: δ 45.2 + 44.1 (2, Me + CH_b), 70.9 (1, CH_a). DMF/CD_3CN (1:1 v/v): δ 44.0 (2), 72.4 (1). $(CD_3)_2SO$: δ 45.5 + 44.6 (2), 70.9 (1).

X-ray Structure Determination. Hexagonal red-black plates of $(Et_4N)_3[Fe_3S_4(LS_3)]$ were grown by vapor diffusion of THF into a DMF solution of the cluster salt. A suitable single crystal was coated with grease and attached to a glass fiber. Diffraction data were collected at −50 °C using a Siemens SMART area diffractometer at Northern Illinois University. Lattice parameters were obtained from least-squares analysis of 100 machine-centered reflections with $10° \le 2\theta \le 20°$. The collected image files were converted to a raw intensity data file using the Siemens SAINT program, and then converted to structure factor amplitudes and their esd's by correction for scan speed, background, and Lorentz and polarization effects using SHELXTL PLUS. The space group was identified by systematic absences. Data collection and crystal parameters are listed in Table 1.

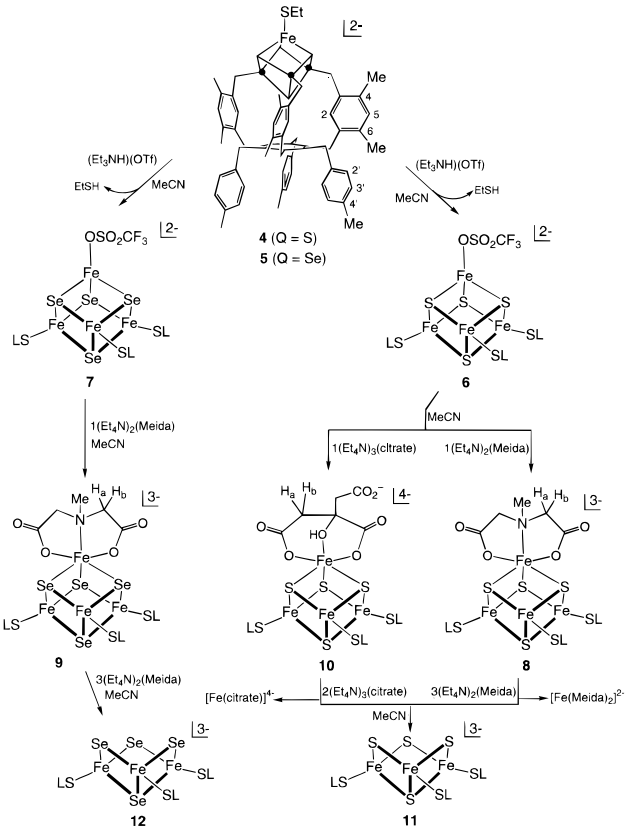

Figure 2. Scheme for the synthesis of Fe_3Q_4 cuboidal clusters **11** and **12** (Q = S, Se); intermediate clusters **6**−**10** have been isolated. The structures of **8**−**10** are consistent with NMR spectra and considered probable in solution. (3LS = LS_3).

Table 1. Crystallographic Data for $(Et_4N)_3[Fe_3S_4(LS_3)]\cdot$MeCN

formula	$C_{77}H_{108}Fe_3N_4S_{13}$
formula wt	1674.13
crystal system	orthorhombic
space group	$P2_12_12_1$
Z	4
a, Å	14.8042(2)
b, Å	18.3989(3)
c, Å	33.1771(2)
V, Å^3	9036.8(2)
ρ_{calc}, g/cm^3	1.328
T, K	223
R,[a] $wR2$[b]	0.0793, 0.1771

[a] $R = \sum||F_o| - |F_c||/\sum|F_o|$. [b] $wR2 = \{\sum[w(F_o^2 - F_c^2)^2]/\sum[w(F_o^2)^2]\}^{1/2}$

The structure was solved by direct methods and was refined by standard least-squares and Fourier techniques. Hydrogen atoms were assigned ideal locations and given the uniform value $B_{iso} = 0.8$ Å^2. The asymmetric unit consists of three cations, one anion, and one acetonitrile solvate molecule. In the last cycle of refinement, all parameters shifted by <1% of their esd's, and the final difference Fourier maps showed no significant electron density. The absolute configuration of the anion was determined by comparison of intensities of Friedel opposite reflections and refinement of the standard absolute configuration (Flack) parameter.[44,45]

Other Physical Measurements. ^{1}H NMR spectra were determined with a Bruker AM 500 spectrometer. Electrochemical measurements were carried out with a PAR Model 263 potentiostat/galvanostat using

(43) Stack, T. D. P.; Weigel, J. A.; Holm, R. H. *Inorg. Chem.* **1990**, *29*, 3745.

(44) Flack, H. D. *Acta Crystallogr.* **1983**, *A39*, 876.

a Pt working electrode and 0.1 M $(Bu_4N)(PF_6)$ supporting electrolyte; potentials are referenced to the SCE. Mössbauer spectroscopic measurements were made utilizing the equipment and techniques described earlier;[46] isomer shifts are quoted relative to Fe metal at room temperature. The program for simulating the integer-spin EPR spectra was written by Dr. M. P. Hendrich at Carnegie Mellon University.

Results and Discussion

Numerous prior attempts in this laboratory to prepare the cuboidal Fe_3S_4 core, nearly all by exposing $[Fe_4S_4]^{2+}$ clusters to oxidizing conditions in the presence or absence of complexing agents to stabilize Fe^{2+}, failed to produce an *isolable* product. Other investigators have provided some evidence for the generation of cuboidal clusters in solution. Weterings *et al*.[47] showed that reaction of $[Fe_4S_4(S\text{-}t\text{Bu})_4]^{2-}$ with $[Fe(CN)_6]^{3-}$ in DMF solution at −40 °C resulted in a 28% conversion to an $[Fe_3S_4]^{1+}$ species, which was identified by Mössbauer and EPR spectroscopies. Subsequently, Roth and Jordanov[48] provided EPR evidence that oxidation of $[Fe_4S_4(Stibt)_4]^{2-}$, containing bulky thiolate ligands, with several different oxidants (including O_2) produced an $[Fe_3S_4]^{1+}$ cluster. Conversion was apparently very low and the product was not stable at room temperature. The low yields and instability of these cluster species suggested that synthetic reactions might better target $[Fe_3S_4]^0$, the other physiological oxidation state of protein-bound clusters (Figure 1). This state is accessible in principle by abstraction of Fe^{2+} from the $[Fe_4S_4]^{2+}$ core, in a process free of the possible complications of redox reactions.

The molecules of particular interest in this work are clusters **4**−**19**. Of these, **4**,[41] **13**,[49] **14** and **15**,[41a,43] **16**,[50] and **17**−**19**[39,51] have been prepared previously. Special note is taken of cubane clusters **16**−**19**. These contain the cuboidal $[Fe_3S_4]^0$ fragment with $S = 2$ which is "spin-isolated" in the cluster because the remaining metal site is diamagnetic.

$[Fe_4Q_4(LS_3)(SEt)]^{2-}$ (Q = S (**4**), Se (**5**))

$[Fe_4Q_4(LS_3)(OSO_2CF_3)]^{2-}$ (Q = S (**6**), Se (**7**))

$[Fe_4Q_4(LS_3)(Meida)]^{3-}$ (Q = S (**8**), Se (**9**))

$[Fe_4S_4(LS_3)(citrate)]^{3-}$ (**10**)

$[Fe_3Q_4(LS_3)]^{3-}$ (Q = S (**11**), Se (**12**))

$[Fe_4S_4(LS_3)(tacn)]^{1-}$ (**13**)

$[Fe_4Q_4(LS_3)Cl]^{2-}$ (Q = S (**14**), Se(**15**))

$[Fe_4S_4(LS_3)(t\text{BuNC})_3]^{1-}$ (**16**)

$[(OC)_3MoFe_4S_4(LS_3)]^{3-}$ (**17**)

$[(OC)_3MoFe_3S_4(SR)_3]^{3-}$ (R = mes (**18**), Et (**19**))

Synthesis of Cuboidal Clusters. In view of the possible instability of the $[Fe_3S_4]^0$ core, we have based our synthetic approach on precursor $[Fe_4Q_4]^{2+}$ clusters coordinated by the semirigid cavitand ligand LS_3,[41a,43] designed to stabilize clusters of trigonal or tetrahedral symmetry. The ligand is sufficiently flexible to bind to both Fe_4S_4[41] and Fe_4Se_4[43] core units, the latter being *ca*. 25% larger than the former when both are in the $[Fe_4Q_4]^{2+}$ oxidation state.[43] We have shown that clusters of the general type $[Fe_4S_4(LS_3)L']^{z-}$ undergo regiospecific substitution at the unique iron subsite,[41,49,50,52] suggesting that other types of reactions may also be localized at this subsite. Clusters **4** and **5** are of this general type; their schematic structures and ligand numbering scheme are shown in Figure 2. Chemical shifts of the isotropically shifted resonances of the 4-Me, 5-H, and 6-Me substituents on the coordinating arms of the ligand are extremely sensitive to the identity of ligand L′,[49,52] a matter that facilitates the monitoring of reactions at the unique subsite. Chemical shifts of substituents (2′-H, 3′-H, 4′-Me) of the buttressing *p*-tolylthio ligand legs are in general much less sensitive to changes in L′. The synthetic scheme affording cuboidal clusters is set out in Figure 2; all reactions were conducted in acetonitrile solutions. Elsewhere we have outlined a second synthetic route based on the removal of the relatively weakly bound $Mo(CO)_3$ group from the cubane cluster **17**.[39] The procedure described below is experimentally more convenient and affords a pure product, free of sodium ion.

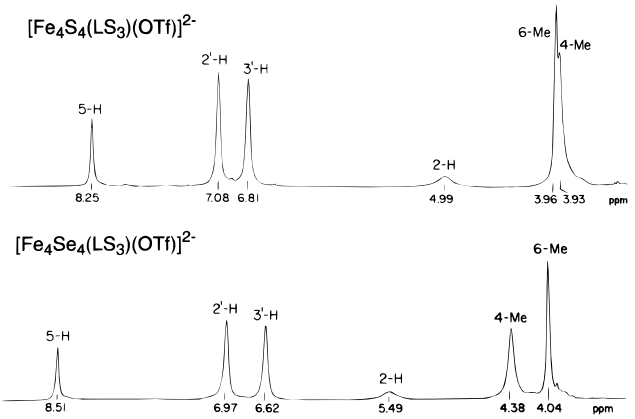

Figure 3. ^{1}H NMR spectra (297 K) of the clusters $[Fe_4Q_4(LS_3)(OSO_2CF_3)]^{2-}$ with Q = S (upper) and Se (lower) in Me_2SO. Signal assignments are indicated; in this and certain other spectra that follow, the 4′-Me signal of LS_3 (near 2.2 ppm) is omitted.

Reaction of cluster **4** with triethylammonium triflate in acetonitrile results in the elimination of ethanethiol and quantitative formation of the triflate-substituted cluster **6**. Its ^{1}H NMR spectrum in Me_2SO, shown in Figure 3, is rather typical of $[Fe_4S_4(LS_3)L']^{2-}$ clusters and is useful for later comparison. Substitution by triflate[53] is demonstrated by elimination of resonances of **4** at 13.1 (SCH_2), 8.13 (5-H), 4.90 (2-H), 3.85 (6-Me), and 3.58 (4-Me) ppm and replacement by those in Figure 3. The presence of triflate activates the unique site toward substitution. Treatment of **6** with 1 equiv of $(Et_4N)_2$(Meida) affords cluster **8**, which was isolated in 95% yield as its Et_4N^+ salt. The cluster was identified by its ^{1}H NMR

(45) See paragraph at the end of this article concerning supporting information available.

(46) Emptage, M. H.; Zimmermann, R.; Que, L., Jr.; Münck, E.; Hamilton, W. D.; Orme-Johnson, W. H. *Biochim. Biophys. Acta* **1977**, *495*, 12.
(47) Weterings, J. P.; Kent, T. A.; Prins, R. *Inorg. Chem.* **1987**, *26*, 324.
(48) Roth, E. K. H.; Jordanov, J. *Inorg. Chem.* **1992**, *31*, 240.
(49) Ciurli, S.; Carrié, M.; Weigel, J. A.; Carney, M. J.; Stack, T. D. P.; Papaefthymiou, G. C.; Holm, R. H. *J. Am. Chem. Soc.* **1990**, *112*, 2654.
(50) Weigel, J. A.; Srivastava, K. K. P.; Day, E. P.; Münck, E.; Holm, R. H. *J. Am. Chem. Soc.* **1990**, 8015.
(51) Coucouvanis, D.; Al-Ahmad, S. A.; Salifoglou, A.; Papaefthymiou, V.; Kostikas, A.; Simopoulos, A. *J. Am. Chem. Soc.* **1992**, *114*, 2472.
(52) Weigel, J. A.; Holm, R. H. *J. Am. Chem. Soc.* **1991**, *113*, 4184.
(53) While we utilize the term "triflate-substituted cluster" and the depictions **6** and **7** for convenience, we cannot demonstrate by NMR whether triflate is actually bound. The ^{19}F chemical shifts of NaOTf and **6** (*ca*. 10 mM in Me_2SO) are the same; this could be the case for bound triflate if spin delocalization to the fluorine atoms were negligible. In any case, a triflate-bound or solvated unique site is expected to be activated relative to the ethanethiolate-bound site in **4**.

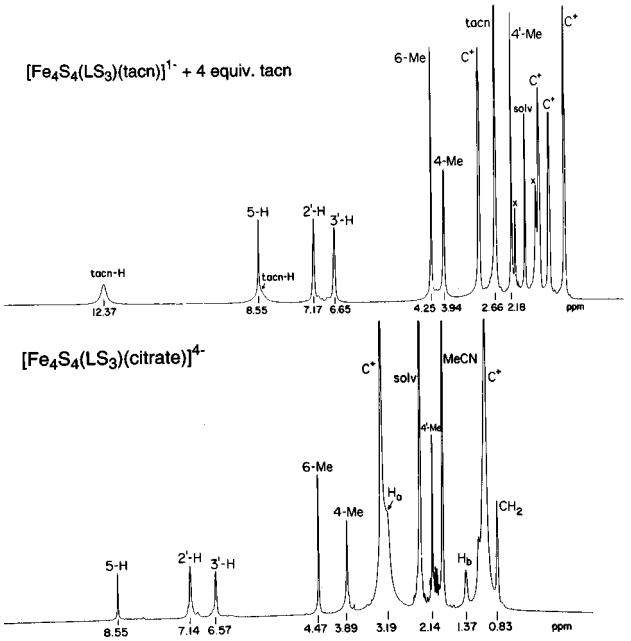

Figure 4. ^{1}H NMR spectra (297 K) of $[Fe_4S_4(LS_3)(tacn)]^{1-}$ + 4 equiv of tacn in Me_2SO (upper) and $[Fe_4S_4(LS_3)(citrate)]^{4-}$ in Me_2SO (lower). Signal assignments are indicated; complete spectra are shown.

spectrum. As demonstrated by structure determinations, Meida[54] (and imidodiacetate[55]) when tridentate strongly favors *fac* stereochemistry, in which protons (H_{ab}) of the same methylene group are inequivalent. Two methylene signals are observed for **8** in Me_2SO at 1.65 and 3.49 ppm (spectrum shown elsewhere[39]). Such methylene proton inequivalence is generally resolved in the spectra of diamagnetic and paramagnetic octahedral *fac* complexes.[56] This cluster also exhibits a 5-H signal at 8.55 ppm; downfield shifts of this resonance past *ca.* 8.25 ppm are frequently empirically associated with 5- or 6-coordination at the unique site.[49] Reaction of **6** with $(Et_4N)_3$(citrate) in acetonitrile afforded the related citrate-bound cluster of proposed structure **10** in 65% yield. The ^{1}H NMR spectrum, presented in Figure 4 (lower), is very similar to that of **8** and shows diastereotopic methylene signals at 1.37 and 3.19 ppm; note also the 5-H resonance at 8.55 ppm, identical to **6**. The indicated coordination mode of citrate is the same as that established in crystalline polymeric $[Fe^{II}(citrate)(OH_2)]^{1-}$ by an X-ray structure analysis.[57]

The reaction of cluster **8** with $n = 1-3$ equiv of $(Et_4N)_2$(Meida) in Me_2SO solution was monitored by ^{1}H NMR as shown in Figure 5. The downfield region, which contains the most information, is presented. At $n = 1$, three new signals appear at 8.51, 11.66, and 15.48 ppm. At $n = 2$, these intensify and the 5-H signal diminishes. The reaction is complete at $n = 3$; signal assignments are made on the basis of relative

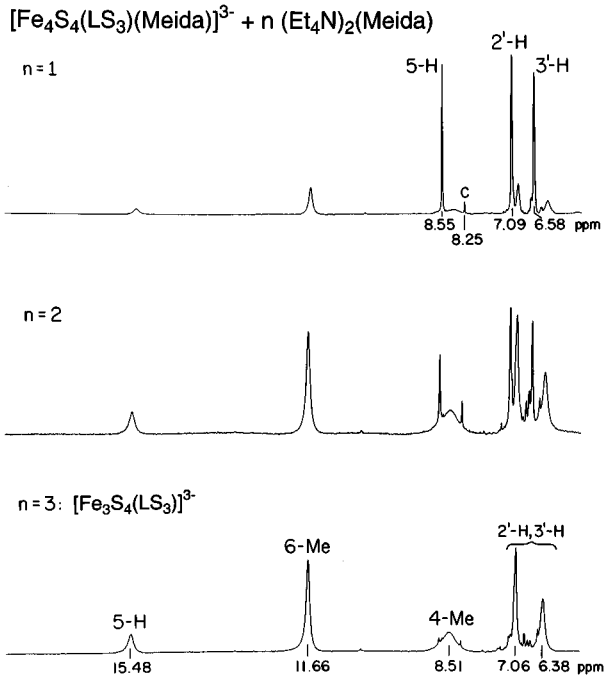

Figure 5. ^{1}H NMR spectra (297 K) demonstrating the reaction of $[Fe_4S_4(LS_3)(Meida)]^{3-}$ with $n = 1-3$ equiv of $(Et_4N)_2$(Meida) in Me_2SO resulting in the formation of the cuboidal cluster $[Fe_3S_4(LS_3)]^{3-}$; signal assignments are indicated.

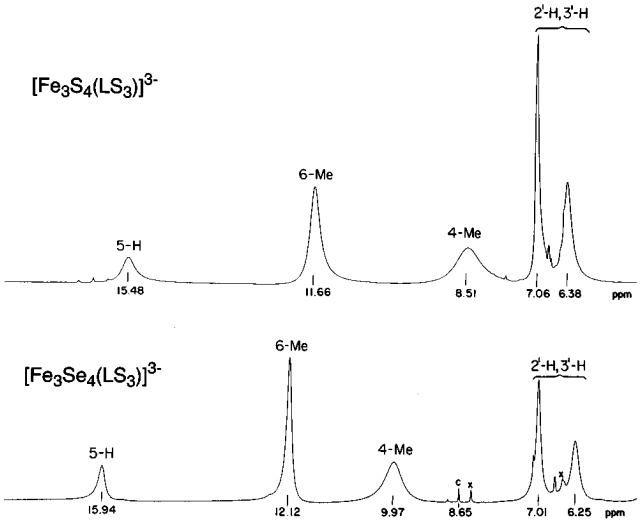

Figure 6. ^{1}H NMR spectra (297 K) of the cuboidal clusters $[Fe_3Q_4(LS_3)]^{3-}$ with Q = S (upper) and Se (lower); signal assignments are indicated.

intensities and line widths, assuming that 4-Me (being closer to the paramagnetic center) will afford a broader line than 6-Me as in the spectra of **4** and **6**. Also reaching maximum intensity at this point are broad features at 45.8 and 71.4 ppm (not shown), identified by relative intensities that arise from Me + CH_b and CH_a, respectively, of $[Fe(Meida)_2]^{2-}$. This complex was independently prepared in solution; the trans-*fac* stereochemistry (one of three possible geometric isomers[56]) is consistent with one set of inequivalent methylene protons in the solution structure. When conducted on a preparative scale, the reaction between **8** and 4 equiv of $(Et_4N)_2$(Meida) in acetonitrile solution afforded the pure product $(Et_4N)_3$[**11**] as black microcrystals in 80% yield. Its ^{1}H NMR spectrum, shown in Figure 6, reveals the same set of downfield-shifted 5-H, 4-Me, and 6-Me signals as in the titration experiments. Because their isotropic shifts are *ca.* 3−5× larger than those of precursor clusters **6** and **8** and the signs of the shifts are consistent with dominant contact

(54) (a) Gheller, S. F.; Hambley, T. W.; Brownlee, R. T. C.; O'Connor, M. J.; Snow, M. R.; Wedd, A. G. *J. Am. Chem. Soc.* **1983**, *105*, 1527. (b) Kushi, Y.; Ideno, T.; Yasui, T.; Yoneda, H. *Bull. Chem. Soc. Jpn.* **1983**, *56*, 2845. (c) Wagner, M. R.; Beach, D. B. *Acta Crystallogr.* **1985**, *C41*, 669. (d) Yamasaki, Y.; Kurisaki, T.; Yamaguchi, T.; Wakita, H. *Acta Crystallogr.* **1993**, *C49*, 229.

(55) (a) Mammano, N. J.; Templeton, D. H.; Zalkin, A. *Acta Crystallogr.* **1977**, *B33*, 1251. (b) Mootz, D.; Wunderlich, H. *Acta Crystallogr.* **1980**, *B36*, 445. (c) Corradi, A. B.; Palmiero, C. G.; Nardelli, M.; Pellinghelli, M. A.; Vidoni Tani, M. E. *J. Chem. Soc., Dalton Trans.* **1973**, 655. (d) Nesterova, Ya. M.; Polynova, T. N.; Porai-Koshits, M. A.; Kramarenko, F. G.; Muratova, N. M. *Zh. Strukt. Khim.* **1979**, *20*, 960.

(56) (a) Cooke, D. W. *Inorg. Chem.* **1966**, *5*, 1141. (b) Smith, B. B.; Sawyer, D. T. *Inorg. Chem.* **1968**, *7*, 922. (c) Pratt, L.; Smith, B. B. *Trans. Faraday Soc.* **1969**, *65*, 915. (d) Erickson, L. E.; Ho, F. F.-L.; Reilley, C. N. *Inorg. Chem.* **1970**, *9*, 1148.

(57) Strouse, J.; Layten, S. W.; Strouse, C. E. *J. Am. Chem. Soc.* **1977**, *99*, 562.

interactions,[58] it follows that the product is substantially more paramagnetic than the cubane clusters. As demonstrated below, species **11** is the desired cuboidal cluster $[Fe_3S_4(LS_3)]^{3-}$, containing the $[Fe_3S_4]^0$ core with an $S = 2$ ground state.

The corresponding cuboidal selenide cluster **12** was prepared in an analogous manner (Figure 2). Cluster **5** was quantitatively converted to the triflate derivative **7**. Reaction of the latter with 1 equiv of $(Et_4N)_2$(Meida) afforded **9**. In several attempts this cluster proved to be difficult to isolate in pure form owing to its tendency to form the cuboidal cluster; it was identified electrochemically (vide infra). Reaction of **7** with 4 equiv of $(Et_4N)_2$(Meida) provided pure $(Et_4N)_3$[**12**] in 87% yield. The ^{1}H NMR spectra of **7** (Figure 3) and **11** (Figure 6) serve to identify these clusters. These species have slightly larger isotropic shifts than their sulfur analogues owing to weaker spin coupling within the core. This property was first discovered with synthetic clusters[42,59] and extends to protein-bound clusters.

The synthetic method is summarized by reaction 1, which when expressed minimally is $[Fe_4Q_4]^{2+} \rightarrow [Fe_3Q_4]^0 + Fe^{2+}$. This is a process of *iron atom abstraction* from a preformed cubane-type $[Fe_4Q_4]^{2+}$ core, for which we are aware of no precedent in iron−chalcogenide cluster chemistry. We next consider several factors responsible for the occurrence of this reaction.

$$[Fe_4S_4(LS_3)(OTf)]^{2-} + 2(Meida)^{2-} \rightarrow [Fe_3S_4(LS_3)]^{3-} + [Fe(Meida)_2]^{2-} + TfO^- \quad (1)$$

Ligand Dependence in Synthesis. The stable existence of cuboidal clusters provokes examination of the factors which promote the abstraction of iron from the cubane precursor and stabilization of the resultant cluster. In order to provide at least a qualitative definition of the features required in the abstracting and stabilizing ligands, we report a series of reactions in which such ligands are varied. Reactions were performed anaerobically and were monitored *in situ* in Me_2SO solutions by ^{1}H NMR spectroscopy.

(a) Abstracting Ligand. Although an extensive study has not been performed, we have examined additional reaction systems to determine the propensity of other multidentate ligands to abstract iron from the core of cluster **6** in Me_2SO solution. When equimolar with **6**, $(EDTA)^{4-}$ effected a quantitative conversion to **11**. Equimolar pyridine-2,6-dicarboxylate (which cannot form a *fac* complex similar to **8**) gave only a 12% yield of **11**. Aconitate, aspartate, bpy, Me_5dien, Me_6tren, and tacn produced no appreciable amount of **11**, although in several cases there was evidence for binding of the ligand to the cluster. Consequently, $(Meida)^{2-}$ is the abstracting ligand of current choice. Although two methylene resonances indicate nonfluxional coordination of the unique iron atom by $(Meida)^{2-}$ in intermediate **8**, one carboxylate must detach at some rate to provide a binding site for the second abstracting ligand enroute to removal of this atom as $[Fe(Meida)_2]^{2-}$. This situation is suggested by the behavior of product cluster **13** in reaction 2;this

$$[Fe_4S_4(LS_3)(OTf)]^{2-} + tacn \rightarrow [Fe_4S_4(LS_3)(tacn)]^{1-} + TfO^- \quad (2)$$

species is formed quantitatively in Me_2SO with 1 equiv of tacn. Its ^{1}H NMR spectrum, shown in Figure 4 (upper) reveals retention of the $S = 0$ ground state of the $[Fe_4S_4]^{2+}$ core, and a downfield-shifted 5-H resonance at 8.55 ppm, accidentally the same as for **8** and **10** and associated with a six-coordinate iron site. In the presence of 4 equiv of tacn in Me_2SO solution, the spectrum of **13** persists unchanged for at least 3 days with no detectable formation of **11**. In contrast, the overall conversions **6** → **11** and **7** → **12** are complete on a preparative scale within 15 min. The putative abstraction products, $[Fe(tacn)_3]^{2+/3+}$, are readily prepared and are kinetically stable,[60] one indication of which is that both are low spin. We conclude that binding of tacn to the unique site is sufficiently tight that the "on" rate of any decoordinated nitrogen atom is so large that a second tacn molecule cannot coordinate at any appreciable rate.

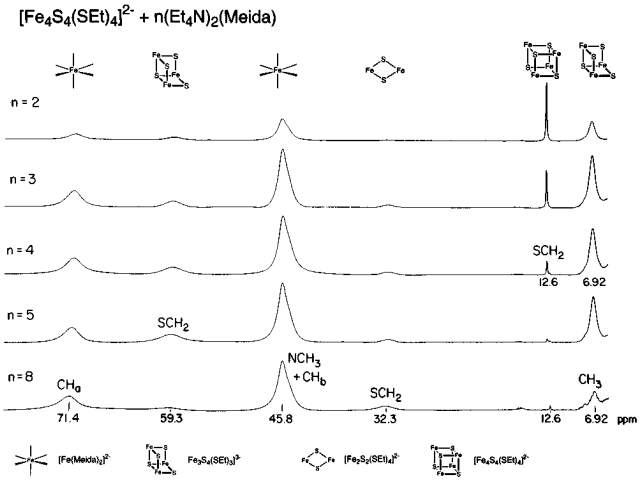

Figure 7. ^{1}H NMR spectra (297 K) of the reaction mixtures $n(Et_4N)_2$(Meida) + $[Fe_4S_4(SEt)_4]^{2-}$ in Me_2SO with $n = 2$, 3, 4, 5, and 8 equiv. Each spectrum was recorded after 30 min reaction time; signal assignments are indicated.

(b) Cluster Ligands. An immediate question is whether the ligand LS_3, whose synthesis[43] is not difficult but requires more than casual effort, is obligatory to the formation and adequate stabilization of cuboidal clusters. This matter has been addressed by examining the products of the reaction systems $n(Et_4N)_2$(Meida)/$(Bu_4N)_2[Fe_4S_4(SEt)_4]$ with $n = 2$, 3, 4, 5, and 8 equiv. The spectrum of each was recorded after 30 min reaction time; the results are set out in Figure 7. At $n = 2$, a partial reaction has occurred, and signals due to $[Fe_4S_4(SEt)_4]^{2-}$ (12.6 ppm) and $[Fe(Meida)_2]^{2-}$ (45.8, 71.4 ppm) are apparent. The remaining signal intensity is found at 59.3 and 6.92 ppm and occurs in a roughly 2:3 intensity ratio. No known all-Fe−S cluster has ethanethiolate resonances at these positions. However, we find that **19**, of proven cubane structure and $S = 2$ ground state,[51] exhibits resonances at 65.5 (CH_2) and 5.97 (CH_3) ppm in Me_2SO. Assuming that isotropic shifts are dominantly contact in origin[61] and thus proportional to magnetic susceptibility, we assign the two similarly shifted signals in the present reaction systems to cuboidal $[Fe_3S_4(SEt)_3]^{3-}$. Of the detectable species, the $n = 2$ system contains 20% unreacted $[Fe_4S_4(SEt)_4]^{2-}$, 31% $[Fe_3S_4(SEt)_3]^{3-}$, and 49% $[Fe(Meida)_2]^{2-}$. At $n \geq 3$, an additional feature at 32.3 ppm from $[Fe_2S_2(SEt)_4]^{2-}$ [35] emerges. At $n = 4$, the relative amount of $[Fe_3S_4(SEt)_3]^{3-}$ maximizes at 36%. At $n = 8$, $[Fe_3S_4(SEt)_3]^{3-} = 19\%$, $[Fe_2S_2(SEt)_4]^{2-} = 9\%$, $[Fe(Meida)_2]^{2-} = 72\%$, and $[Fe_4S_4(SEt)_4]^{2-}$ is barely detectable.[62]

(58) $(\Delta H/H_0)_{iso} = (\Delta H/H_0)_{dia} - (\Delta H/H_0)_{obs}$; contact interactions require that 4-Me, 5-H, and 6-Me shifts have the same sign.[38b]

(59) (a) Bobrik, M. A.; Laskowski, E.; Johnson, R. W.; Gillum, W. O.; Berg, J. M.; Hodgson, K. O.; Holm, R. H. *Inorg. Chem.* **1978**, *17*, 1402. (b) Reynolds, J. G.; Coyle, C. L.; Holm, R. H. *J. Am. Chem. Soc.* **1980**, *102*, 4350. (c) Reynolds, J. G.; Holm, R. H. *Inorg. Chem.* **1980**, *19*, 3257.

(60) (a) Wieghardt, K.; Schmidt, W.; Herrmann, W.; Küppers, H.-J. *Inorg. Chem.* **1983**, *22*, 2953. (b) Boeyens, J. C. A.; Forbes, A. G. S.; Hancock, R. D.; Wieghardt, K. *Inorg. Chem.* **1985**, *24*, 2926.

(61) This property is reasonably demonstrated by the negative isotropic shifts of the methylene and methyl groups in the ratio 14:1, and the signs of shifts of phenyl-based ligands[39,51] which are indicative of π-delocalization of spin.

While a cuboidal cluster with conventional terminal ligands can be formed, the reaction of $[Fe_4S_4(SEt)_4]^{2-}$ with $(Meida)^{2-}$ is incomplete under conditions ($n = 3$, 4) where that of **6** produces **11** in 80% isolated yield. Further, the proportion of $[Fe(Meida)_2]^{2-}$ always exceeds that of $[Fe_3S_4(SEt)_3]^{3-}$ (by 16−53% at $n = 2-8$), indicating that $(Meida)^{2-}$ abstracts iron from species other than $[Fe_4S_4(SEt)_4]^{2-}$. The source of complexity in these reaction systems does not arise solely from the requirement of removing ethanethiolate from the abstractable iron site. Reaction 3 of thiolate cluster **4** affords a >90% *in*

$$[Fe_4S_4(LS_3)(SEt)]^{2-} + 2(Meida)^{2-} \rightarrow [Fe_3S_4(LS_3)]^{3-} + [Fe(Meida)_2]^{2-} + EtS^- \quad (3)$$

situ conversion to **11** with 4 equiv of abstracting ligand; several unidentified signals are observed in the 6−7 ppm region but there is no indication of the formation of another paramagnetic cluster type. On a preparative basis, triflate cluster **6** leads to a purer product, and thus is the preferred precursor to the cuboidal cluster.

(c) Stability. We have previously shown that the reaction of $[Fe_4S_4(LS_3)(S\text{-}t\text{-}Bu)]^{2-}$ with >4 equiv of *t*-BuSNa in Me_2SO resulted in decoordination of the LS_3 ligand and formation of $[Fe_4S_4(StBu)_4]^{2-}$ in high yield.[41a] In this work, a similar reaction 4 of **4** with NaSEt afforded quantitative formation of the cubane product. The analogous reaction 5 proceeds,

$$[Fe_4S_4(LS_3)(SEt)]^{2-} + 3NaSEt \rightarrow [Fe_4S_4(SEt)_4]^{2-} + Na_3(LS_3) \quad (4)$$

$$[Fe_3S_4(LS_3)]^{3-} + 3NaSEt \rightarrow [Fe_3S_4(SEt)_3]^{3-} + Na_3(LS_3) \quad (5)$$

although not stoichiometrically, and provides a means of studying the stability of the product cuboidal clusters. A solution of **11** (6.1 μmol in 0.5 mL) was treated with a solution of NaSEt (30 μmol in 0.1 mL). A spectrum taken at 10 min reaction time showed the relative percentages of the cluster products to be 65% $[Fe_3S_4(SEt)_3]^{3-}$ and 35% $[Fe_4S_4(SEt)_4]^{2-}$; no starting cluster remained. After 1 h, these amounts decreased and increased by 10%, respectively, and a trace amount of $[Fe_2S_2(SEt)_4]^{2-}$ appeared. At 1−50 h, the direction of these changes continued and a small quantity of linear $[Fe_3S_4(SEt)_4]^{3-}$ appeared and decayed, until at 50 h there remained 11% $[Fe_3S_4(SEt)_3]^{3-}$, 35% $[Fe_2S_2(SEt)_4]^{2-}$, and 54% $[Fe_4S_4(SEt)_4]^{2-}$. The means of formation of the non-cuboidal clusters is obscure. What is evident, however, is that $[Fe_3S_4(SEt)_3]^{3-}$, in the presence of bi-, tri-, and tetranuclear clusters which may be derived from it, is moderately unstable and decays to known clusters. This cluster appears sufficiently stable to be isolable, but under conditions requiring separation from other clusters. We have not observed formation of $[Fe_3S_4(SEt)_3]^{3-}$, by reactions 3 or 5 or any other means, without accompanying formation of other cluster(s). Cluster **11** is stable for at least 1 week, and **12** for 2−3 days, in anaerobic solutions at ambient temperature. Thus, the auspicious effect of the LS_3 ligand system in promoting both the formation and stability of the $[Fe_3S_4]^0$ core is demonstrated.

(62) Because of large line widths of most resonances, percentages of species obtained by integration in this and related experiments are semiquantitative only.

(63) Carney, M. J.; Papaefthymiou, G. C.; Spartalian, K.; Frankel, R. B.; Holm, R. H. *J. Am. Chem. Soc.* **1988**, *110*, 6084 and references therein.

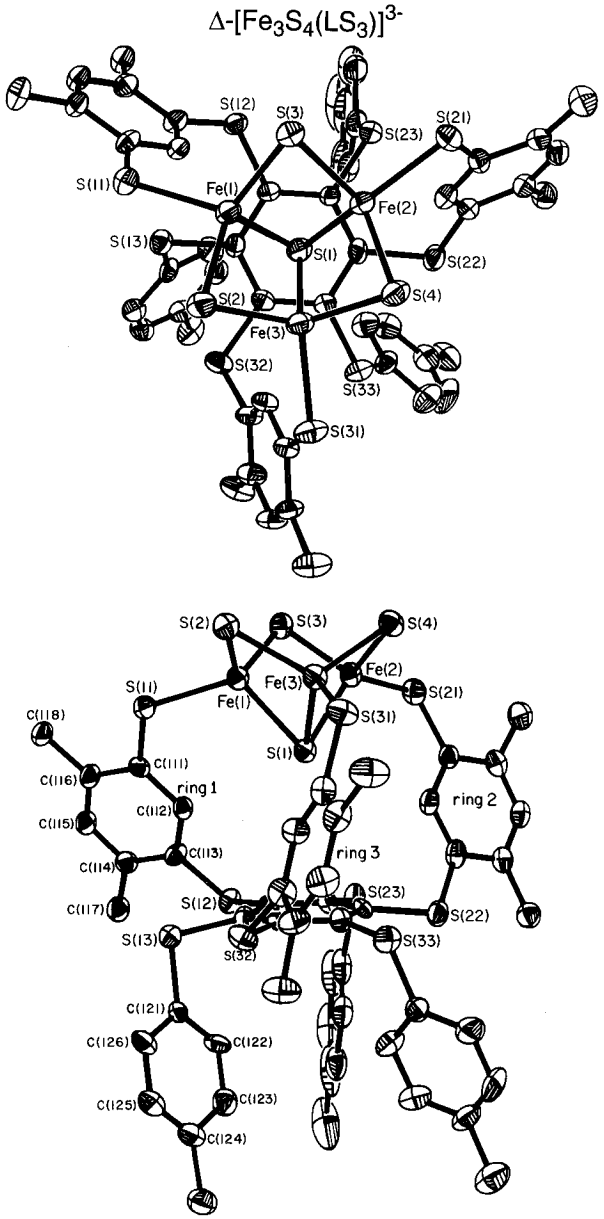

Figure 8. Structure of $[Fe_3S_4(LS_3)]^{3-}$ as its Et_4N^+ salt, showing the atom numbering scheme for Fe and S atoms and for one ligand arm and leg, and 50% probability ellipsoids. Lower: Perspective view of the entire structure roughly perpendicular to the idealized C_3 axis, which contains S(1) and bisects the central benzene ring carrying S(13,23,-33). Upper: View along the idealized C_3 axis emphasizing the Δ absolute configuration.[43]

Cluster Reconstitution. As a further structure proof in solution, we have demonstrated that reaction 6 proceeds

$$[Fe_3Q_4(LS_3)]^{3-} + [FeCl_4]^{2-} \rightarrow [Fe_4Q_4(LS_3)Cl]^{2-} + 3Cl^- \quad (6)$$

quantitatively in Me_2SO to yield the chloride clusters with the following chemical shifts: **14**, 3.79 (4-Me), 3.90 (6-Me), 8.22 (5-H); **15**, 4.28 (4-Me), 4.04 (6-Me), 8.48 (5-H). The values are identical with those of the authentic clusters[41a,43] in the same solvent. The minimal reaction is the reverse of preparative reaction 1, *viz*. $[Fe_3Q_4]^0 + Fe^{2+} \rightarrow [Fe_4Q_4]^{2+}$.

Solid State Structure of $[Fe_3S_4(LS_3)]^{3-}$. The compound $(Et_4N)_3$[**11**]·MeCN crystallizes in an orthorhombic space group with no imposed symmetry. Two views of the structure of the entire anion are available in Figure 8 and the core structure is shown in more detail in Figure 9. It is immediately evident

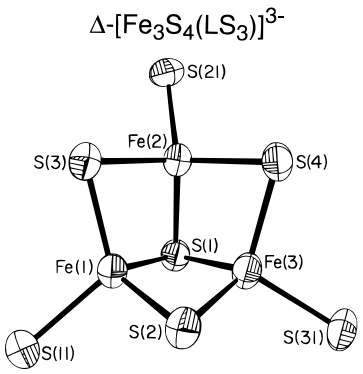

Figure 9. Structure of the $[Fe_3S_4]^0$ core of $[Fe_3S_4(LS_3)]^{3-}$, with 50% probability ellipsoids and the atom labeling scheme.

Table 2. Selected Interatomic Distances (Å) and Angles (deg) for $[Fe_3S_4(LS_3)]^{3-}$

Fe(1)−S(1)	2.310(2)	Fe(1)−Fe(2)	2.712(2)
Fe(2)−S(1)	2.273(3)	Fe(1)−Fe(3)	2.665(2)
Fe(3)−S(1)	2.333(2)	Fe(2)−Fe(3)	2.731(2)
mean of 3	2.31(3)	mean of 3	2.70(3)
Fe(1)−S(2)	2.274(2)	Fe(1)−S(11)	2.316(3)
Fe(1)−S(3)	2.251(3)	Fe(2)−S(21)	2.310(3)
Fe(2)−S(3)	2.242(2)	Fe(3)−S(31)	2.327(3)
Fe(2)−S(4)	2.265(3)	mean of 3	2.318(9)
Fe(3)−S(4)	2.250(3)		
Fe(3)−S(2)	2.275(3)	S(11)−C(111)	1.746(8)
mean of 6	2.26(2)	S(21)−C(211)	1.774(9)
		S(31)−C(311)	1.746(10)
		mean of 3	1.76(2)
Fe(2)−S(1)−Fe(1)	72.56(8)	Fe(3)−Fe(1)−Fe(2)	61.03(4)
Fe(2)−S(1)−Fe(3)	72.70(8)	Fe(1)−Fe(3)−Fe(2)	60.34(4)
Fe(1)−S(1)−Fe(3)	70.05(7)	Fe(1)−Fe(2)−Fe(3)	58.63(4)
S(2)−Fe(1)−S(3)	112.5(1)	Fe(1)−S(3)−Fe(2)	74.27(8)
S(3)−Fe(2)−S(4)	111.5(1)	Fe(2)−S(4)−Fe(3)	74.42(8)
S(4)−Fe(3)−S(2)	113.8(1)	Fe(3)−S(2)−Fe(1)	71.71(8)
S(2)−Fe(1)−S(1)	106.06(9)		
S(3)−Fe(1)−S(1)	102.17(9)		
S(3)−Fe(2)−S(1)	103.59(10)		
S(4)−Fe(2)−S(1)	103.02(9)		
S(4)−Fe(3)−S(1)	101.63(9)		
S(2)−Fe(3)−S(1)	105.27(9)		

that the desired cuboidal cluster has been achieved. The structures of only two other LS_3 clusters have been determined, $(Ph_4P)_2$[**14**][41a] and $(Ph_4P)_2$[**15**]·2DMF;[43] both have a common chloride ligand at the unique site. The latter crystallizes in trigonal space group *P*3 with three one-third anions in the asymmetric unit. We shall have occasion to compare the present structure with these.

(a) Conformation. We have developed a conformational analysis for substituted benzenes whose phenyl substituents are connected to the central ring (ring 0) by one atom.[41a] The molecular conformation of **11** is describable at two levels. First, the cluster is found in the *ababab* conformation, in which alternate phenylthio substitutents are above and below the plane of ring 0. The three ligand arms with rings 1−3 coordinate the Fe_3S_4 core with atoms S(11,21,31), and are buttressed into position by the three *p*-tolylthio legs. The six connecting sulfur atoms of ring 0 are below it (away from the core) at a mean distance of 0.19 Å. This displacement contributes to the placement of S(1) at 3.77 Å above the center of ring 0, compared to 3.74 Å for **14**. The van der Waals contact distance between ring 0 and S(1) is estimated to be 3.44 Å. The core substantially occupies the ligand cavity whose walls are defined by the inward edges of rings 1−3. At a second level, the conformation is quantitatively described by the dihedral angles in Table 3. the inequality within each set of the angles ψ between ring 0 and

Table 3. Conformational Analysis of $[Fe_3S_4(LS_3)]^{3-}$ (deg)[a]

conformation	ring	ψ (ring 0/ring *n*)	θ (tilt)	ϕ (cant)
ababab	1	66.63	51.88	27.74
	2	69.62	44.28	44.04
	3	70.42	52.96	30.87
	4	106.76	−85.19	−46.91
	5	105.53	−64.29	−20.59
	6	97.59	−71.10	−31.96

[a] Tilt and cant angles are defined by the dihedral angles formed by the shaded atoms relative to a planar reference conformation with $\theta = \phi = 0°$.

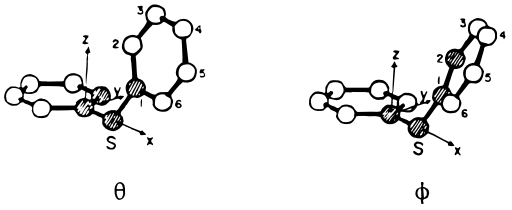

rings 1−3 (arms) and rings 4−6 (legs) is the simplest indication that the ligand conformation lacks C_3 symmetry. The conformation is precisely described by the angles θ (tilt) and ϕ (cant), which also indicate departure from trigonal symmetry and convey the orientation of rings 1−6 with respect to ring 0. The binding of the cuboidal core to the ligand renders the cluster chiral. However, the sign of neither the tilt nor cant angle necessarily correlates with absolute configuration. Given the criteria developed previously,[43] the absolute configuration of the cluster in the crystal of $(Et_4N)_3$[**11**]·MeCN examined is Δ. A clockwise trigonal twist about the idealized C_3 axis viewed from the *S*(2−4) core face recovers the Λ enantiomer. Earlier, cluster **15** was found in an inversion-twinned crystal with the ratio Δ:Λ = 2:1.[43]

(b) Core. Under idealized C_{3v} symmetry, the bond distances and angles of a cuboidal Fe_3S_4 divide into 3 + 6Fe−S, 3Fe−Fe, (3 + 3)Fe−S−Fe, (3 + 6)S−Fe−S, and 3Fe−Fe−Fe. Metric data are arranged in this manner in Table 2. The data reveal departures from this symmetry in a manner suggestive of a pseudomirror plane containing atoms Fe(2), S(1), and S(2). Bond distances and angles are unexceptional for Fe−S clusters. The most interesting structural aspect is the relationship between the cubane and cuboidal cores, where the issue is the extent of change when an iron atom is in actuality removed from the former to generate the latter. For this purpose, we take **14** as the reference. Mean values of independent structural parameters for the $[Fe_3S_4]^0$ core of **11** and the $[Fe_4S_4]^{2+}$ core of **14** are compared in Figure 10. The latter lacks the elongated tetragonal distortion common to such cores[34a,63] and instead approaches T_d symmetry, under which its metric data have been averaged. The absent iron atom in the depiction is understood to be that at the unique site. The comparison, made in terms of mean values of angles and distances, carries the caveat that the mean iron oxidation states of the cores differ ($Fe^{2.67+}$ in **11**, $Fe^{2.50+}$ in **14**). Given this difference, we are unable to explain why the terminal Fe−S distances are longer in **11** (2.32 Å) than in **14** (2.26 Å). With almost no exceptions, bond lengths decrease as the oxidation state increases in the series $[Fe_4S_4]^{1+,2+,3+}$,[34a,64] i.e., as the Fe^{3+} character of the core increases.[65]

Removal of an iron atom from a cubane core might be expected to cause relaxation of the structure to a more open, or splayed, configuration. In this case, the remaining μ_3-S atom would experience increased Fe−S(1)−Fe bond angles and the three S−Fe−S angles would expand. Evidence for this effect

(64) (a) O'Sullivan, T.; Millar, M. M. *J. Am. Chem. Soc.* **1985**, *107*, 4096. (b) Carney, M. J.; Papaefthymiou, G. C.; Frankel, R. B.; Holm, R. H. *Inorg. Chem.* **1989**, *28*, 1497 and references therein.

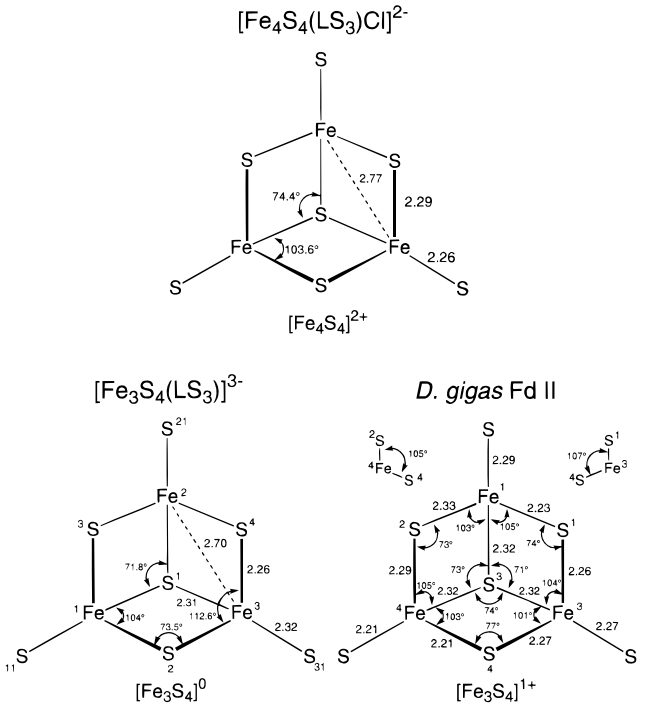

Figure 10. Metric features of the core structures of $[Fe_4S_4(LS_3)Cl]^{2-}$ [41a] (mean bond distances and angles averaged under idealized T_d symmetry; one Fe atom removed from core), $[Fe_3S_4(LS_3)]^{3-}$ (mean bond distances and angles averaged under idealized C_{3v} symmetry), and *D. gigas* Fd II.[5b] The small numbers correspond to the atom labeling scheme of Figure 9 and of the protein structure. Certain angles are shown outside the protein cluster, which is depicted after Kissinger *et al*.[5]

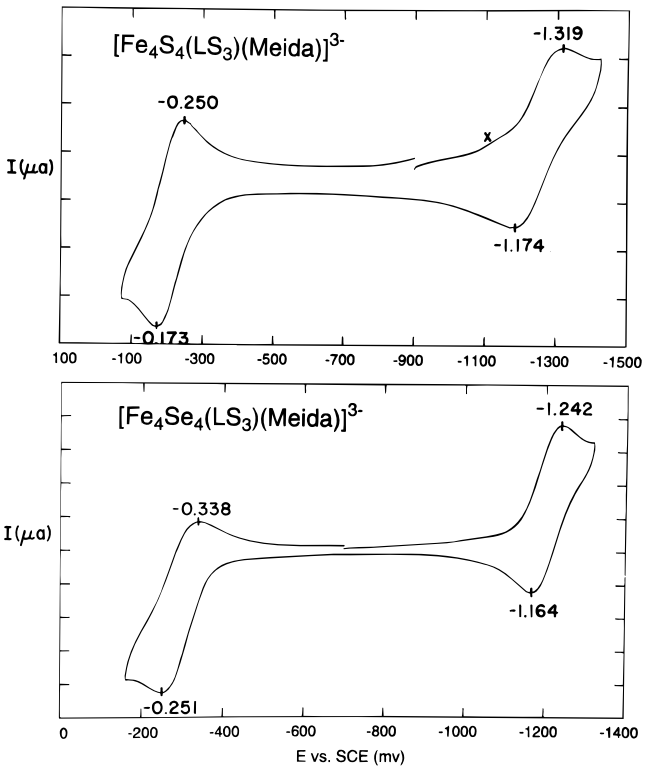

Figure 11. Cyclic voltammograms (50 mV/s) of $[Fe_4Q_4(LS_3)(Meida)]^{3-}$ in acetonitrile with Q = S (upper) and Se (lower). Peak potentials are indicated; x = slight impurity of $[Fe_4S_4(LS_3)(OSO_2CF_3)]^{2-}$.

is found in the S−Fe−S angle of 112.6° vs 103.6° in the cubane core. The angles at μ_3-S have contracted by a small amount (2.6°) in passing to the cuboidal form. Overall, the cubane and cuboidal cores are closely related metrically. Other than the 9.0° angle increase noted, the principal dimensional difference in the two cores is the 0.07-Å decrease in Fe−Fe separations in forming the cuboidal species. The average values of all Fe−S distances in the two cores are indistinguishable (2.28, 2.29 Å). These bond lengths are symmetry-differentiated in the cuboidal core where, as expected, Fe−(μ_2-S) bonds are shorter than Fe−(μ_3-S) bonds (by 0.05 Å).

In the structure of oxidized *Av* Fd I, the reported average values Fe−Fe = 2.68 Å and Fe−(μ_3-S)−Fe = 70.5° [6a] are close to the corresponding values in **11** (2.70 Å, 71.8°). The structure of this protein has also been determined in the oxidized and dithionite-reduced ($[Fe_3S_4]^0$) forms at pH 8 and 6.[6c] The cluster structure is the same in the four structures, with some evidence adduced for protonation of the reduced form at acid pH. Explicit dimensional data for reduced clusters were not reported. Included in Figure 10 are the distance and angle data for the $[Fe_3S_4]^{1+}$ core of *Dg* Fd II.[5b] These data were not averaged because of the large spread in certain parameters that would be identical under trigonal symmetry. Despite core distortions and a different oxidation state, it is clearly evident that structures of the synthetic and protein-bound cores are substantially the same. Kissinger *et al*.[5] have emphasized the close dimensional relationship between the *Dg* Fd II cluster and those of typical Fd proteins in the $[Fe_4S_4]^{2+}$ state. Stout[6a] has concluded that "there is no distinguishable difference" between the $[Fe_3S_4]^{1+}$ and $[Fe_4S_4]^{2+}$ clusters of *Av* Fd I except for the number of atoms. The lack of a major structural change contributes to the facility of removal of Fe^{2+} from the cubane core and the ready reconstitution of the core in reaction 6. The same point applies to the binding of extrinsic metal ions to the synthetic[39] and protein-bound[7,10,36,37] cores to afford the heterometal cubane-type MFe_3S_4 clusters.

Electron Transfer Reactions. Relevant electron transfer series and redox potentials are collected in Table 4. Unless noted otherwise, the processes are chemically reversible ($i_{pa}/i_{pc} \approx 1$) one-electron reactions. Shown in Figure 11 are cyclic voltammograms of the two immediate precursors to the cuboidal clusters, the cubanes **8** and **9**, which exhibit the three-membered series 7. The less negative potential for reduction of $[Fe_4Se_4]^{2+}$ clusters is precedented.[42,59a] Amongst LS_3 species this property is further illustrated by the values for **14** and **15** in DMF, which differ by 80 mV. The more negative potentials for **8** and **9** are most likely due to their 3− charge. The conversions **8** → **11** and **9** → **12** afford cuboidal clusters that manifest the chemically reversible, three-membered electron transfer series 8; these processes approach (at 50 mV/s) the criterion $\Delta E_p = 59$ mV for an electrochemically reversible one-electron reaction.

Although of equal overall charge, the potentials of **11/12**, shown in the voltammograms of Figure 12, are considerably more negative than those of **8/9**, an effect we ascribe to the differences in *core* charges in the two sets of clusters. For example, on a charge basis it should be more difficult to reduce a $[Fe_3S_4]^0$ than a $[Fe_4S_4]^{2+}$ core at near-parity of terminal ligation. Inasmuch as the $[Fe_3S_4]^{1+,0}$ states are known in proteins and $[Fe_3S_4]^0$ has now been synthesized, the most interesting result is the generation of the $[Fe_3S_4]^{1-}$ state, detected for the first time in the absence of a stabilizing cation as in certain heterometal cubanes **3**. The decidedly negative potential for the formation of this oxidation state is suggestive of the need for cluster protonation in stabilization of the protein-bound

(65) It has not escaped our attention that the pattern of Fe−Fe separations in **11** (Table 2) is such as to approximate an isosceles triangle. On the basis of this pseudosymmetry, Fe(1,3) would be the delocalized pair and Fe(2) the Fe^{3+} site. However, the Fe−Fe distances themselves are not necessarily consistent with this picture. Further, the terminal Fe−S bond lengths, which are generally sensitive to the oxidation states of the Fe atom in Fe−S clusters as noted above, cover a range of ≲0.02 Å, and thus do not reflect differences in oxidation states. Additional structures of $[Fe_3S_4]^0$ clusters are being sought to examine the relationship between metric features and electronic structure.

Table 4. Cluster Electron Transfer Series and Redox Potentials

cluster	solvent	series	$E_{1/2}$, V[a] 0/1−	1−/2−	2−/3−	3−/4−
$[Fe_4S_4(LS_3)(Meida)]^{3-}$ (**8**)	MeCN	(7a)		−0.21	−1.25	
$[Fe_4Se_4(LS_3)(Meida)]^{3-}$ (**9**)	MeCN	(7b)		−0.27	−1.20	
$[Fe_4S_4(LS_3)Cl]^{2-}$ (**14**)	DMF				−1.03	
	CH_2Cl_2[b]			+0.12	−1.08	
$[Fe_4Se_4(LS_3)Cl]^{2-}$ (**15**)	DMF				−0.95	
$[Fe_3S_4(LS_3)]^{3-}$ (**11**)	MeCN	(8a)			−0.79	−1.72
$[Fe_3Se_4(LS_3)]^{3-}$ (**12**)	MeCN	(8b)			−0.80	−1.67
$[Fe_4S_4(LS_3)(t\text{-BuNC})]^{1-}$ (**16**)	CH_2Cl_2[b]	(9)	−0.18	−1.08		
$[(OC)_3MoFe_3S_4(LS_3)]^{3-}$ (**17**)	MeCN	(10a)			∼−0.20[c]	−0.78
$[(OC)_3MoFe_3S_4(Smes)_3]^{3-}$ (**18**)	MeCN	(10b)			−0.31	−0.86
$[(OC)_3MoFe_3S_4(SEt)_3]^{3-}$ (**19**)[d]	CH_2Cl_2	(10c)			−0.40	−0.94

[a] 298 K, vs SCE. $E_{1/2} = (E_{pc} + E_{pa})/2$. [b] Reference 50. [c] Poorly defined feature. [d] For additional data on clusters of this type, *cf.* ref 51.

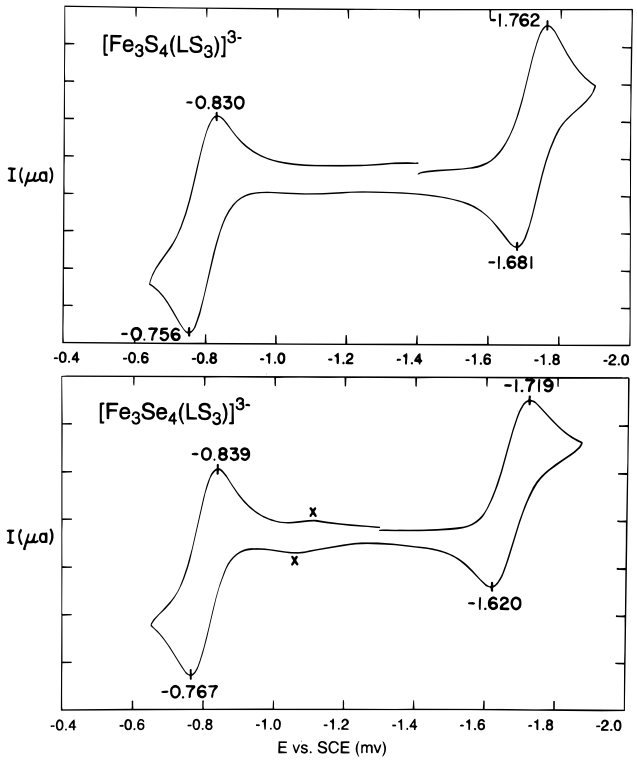

Figure 12. Cyclic voltammograms (50 mV/s) of $[Fe_3Q_4(LS_3)]^{3-}$ in acetonitrile with Q = S (upper) and Se (lower). Peak potentials are indicated; x = impurity.

$[Fe_3S_4]^{1-,2-}$ states at accessible potentials in water (Figure 1). Electron transfer series 9 and 10 based on spin-isolated clusters **16**−**19** cover at least the $[Fe_3S_4]^{0,1-}$ core oxidation states that are traversed in series 8a. The site of oxidation is perhaps ambiguous and could be either the cuboidal fragment or low-spin Fe(II) (**16**) or Mo(O) (**17**−**19**). However, reduction potentials larger than *ca.* −1.0 V are not reasonably assignable to such sites. At parity of overall charge in series 8a and 10, stabilization of the $[Fe_3S_4]^{1-}$ state is quite evident. The most exact comparison is with **11** and **17**, for which the stabilization is 0.94 V in acetonitrile. We find this value unexpectedly large, given that in the analogous clusters **18**[39] and **19**,[51] X-ray structural results clearly show that the $Mo(CO)_3$ group is weakly bonded to the $[Fe_3S_4]^0$ fragment. Series 10b closely approaches electrochemical reversibility; its most reduced member is a potential source of the $[Fe_3S_4]^{1-}$ core without LS_3 stabilization by displacement of $Mo(CO)_3$ and trapping with metal ions.

Mössbauer Spectroscopy and Electronic Structure. Before presenting data pertinent to electronic structure, we summarize briefly the salient features of the Mössbauer spectra of protein-bound $[Fe_3Q_4]^0$ clusters.[2,3,13,26,28,40,66−68] Mössbauer spectra recorded in the absence of an applied magnetic field consist of two quadrupole doublets with intensity ratio 2:1. The less intense doublet typically has an isomer shift, $\delta = 0.30-0.35$ mm/s, slightly larger than those observed for a ferric site with tetrahedral sulfur coordination, while the more intense doublet has a shift, $\delta = 0.46-0.49$ mm/s, suggestive of a valence-delocalized $Fe^{2+}Fe^{3+}$ pair. In the presence of applied magnetic fields, the low-temperature Mössbauer spectra display intricate and well-resolved magnetic patterns whose features reflect the properties of an $S = 2$ spin system with zero-field splitting parameters $D \approx -2.5$ cm^{-1} and $E/D = 0.20-0.25$. The spectra have been analyzed with the spin Hamiltonian 7 (for details, see ref 13), where the quadrupole interactions are given by eq 8. The electron spin S is the cluster spin, D and E are the axial

$$H = D\left[S_z^2 - \frac{1}{3}S(S+1) + \frac{E}{D}(S_x^2 - S_y^2)\right] + \beta \boldsymbol{H}\cdot\boldsymbol{g}\cdot\boldsymbol{S} + \sum_{i=1}^{3}[\boldsymbol{S}\cdot\boldsymbol{A}(i)\cdot\boldsymbol{I}(i) - g_n\beta_n\boldsymbol{H}\cdot\boldsymbol{I}(i) + H_Q(i)] \quad (7)$$

$$H_Q(i) = \frac{eQV_{\zeta\zeta}(i)}{12}\{3\boldsymbol{I}_\zeta^2(i) - I(I+1) + \eta(i)[\boldsymbol{I}_\xi^2(i) - \boldsymbol{I}_\eta^2(i)]\} \quad (8)$$

and rhombic zero-field splitting parameters, respectively, and **g** is the electronic **g** tensor. The magnetic hyperfine interactions of the three sites of an $[Fe_3S_4]^0$ cluster are described by the tensors $\mathbf{A}(i)$, where $i = 1, 2, 3$ sums over the three iron sites. We have found that the ζ-axes of the electric field gradient tensors (principal axes components $V_{\xi\xi}$, $V_{\eta\eta}$, $V_{\zeta\zeta}$) of the individual sites are rotated relative to the z-axis of the zero-field splitting tensor, and we describe this rotation by the polar angle β. At 4.2 K, the electronic spins of all the Fe_3S_4 clusters studied to date relax slowly on the time scale of Mössbauer spectroscopy (≈10 MHz). Under these conditions, the salient features of the low-temperature spectra are determined by the expectation value of the spin of the lowest electronic level. A plot of $\langle S_i \rangle$ along the principal axes of the ZFS tensor shown in Figure 13 suggests the strategy to be used for the analysis of the spectra. Thus, at low field $\langle S_z \rangle$ saturates readily at $\langle S_z \rangle = -2$, while $\langle S_x \rangle$ and $\langle S_y \rangle$ remain small. Consequently, the low-field ($H < 2.0$ T) spectra of each iron site are dominated by the magnetic hyperfine field along z, $H_{int}(i) = -\langle S_z \rangle A_z(i)/g_n\beta_n$, and by the component of the electric field gradient tensor along

(66) Surerus, K. K.; Chen, M.; van der Zwaan, W.; Rusnak, F. M.; Kolk, M.; Duin, E. C.; Albracht, S. P. J.; Münck, E. *Biochemistry* **1994**, *33*, 4980.
(67) Hu, Z.; Jollie, D.; Burgess, B. K.; Stephens, P. E.; Münck, E. *Biochemistry* **1994**, *33*, 14475.
(68) Teixeira, M.; Moura, I.; Xavier, A. V.; Moura, J. J. G.; LeGall, J.; DerVartanian, D. V.; Peck, H. D., Jr.; Huynh, B. H. *J. Biol. Chem.* **1989**, *264*, 16435.

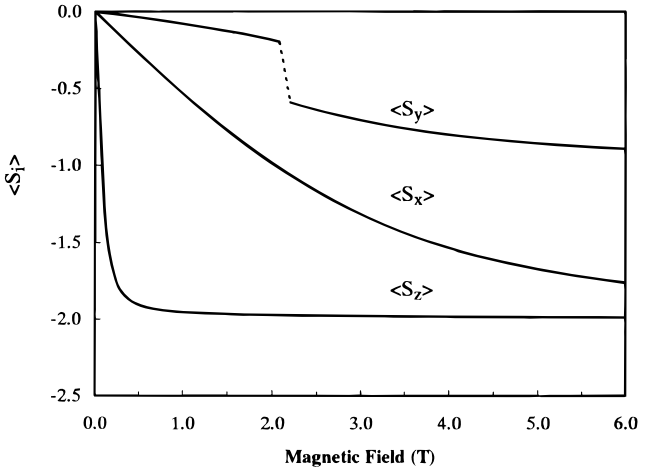

Figure 13. Plot of $\langle S_x\rangle$, $\langle S_y\rangle$, and $\langle S_z\rangle$ for the lowest electronic level of the $S = 2$ system for $D = -2.5$ cm^{-1}, $E/D = 0.25$, and $g_x = g_y = g_z = 2.0$. $\langle S_x\rangle$ is the expectation value of S with the magnetic field applied along the x-direction. The jump in $\langle S_y\rangle$ reflects a level crossing.

H_{int}. As the applied field is increased, the x and y components of the **A** tensors become important. By following the increase of the magnetic hyperfine field with increasing applied field, the ZFS parameters D and E/D can be determined. Thus, by a judicious choice of experimental conditions, a substantial number of fine structure and hyperfine structure parameters can be determined with good precision. Finally, since the g-values of eq 7 are close to $g = 2$, the Mössbauer spectra are quite insensitive to g.

Figures 14D and 14B show 4.2 K zero-field Mössbauer spectra of clusters **11** and **12**, respectively. For comparison, the corresponding spectrum of *Dg* Fd II is shown in Figure 14C. The spectra of the synthetic clusters exhibit intensity patterns essentially identical with those observed for proteins containing the $[Fe_3S_4]^0$ [26−28] and $[Fe_3Se_4]^0$ [40] clusters. By using a Fourier transform deconvolution[69] that removes the line width contribution of the ^{57}Co source, one can frequently improve the resolution of the Mössbauer spectra. As can be seen from the spectrum of Figure 14A, application of this technique to the spectrum of Figure 14B shows that the quadrupole splittings and isomer shifts of the sites P2 and P3 (the delocalized Fe^{2+}-Fe^{3+} pair) differ slightly. The solid lines in Figures 14B and 14D are least-squares fits that yielded the parameters for ΔE_Q and δ listed in Table 5.[70]

As outlined for the analysis of *Dg* Fd II,[13] the ground state of the $[Fe_3S_4]^0$ cluster has an electron configuration consisting of a valence-delocalized $Fe^{2+}Fe^{3+}$ pair and a trapped-valence Fe^{3+} site. The Mössbauer study of *Dg* Fd II has also revealed an excited configuration, X, that becomes populated at temperatures above 25 K. Configuration X, represented by one quadrupole doublet with $\Delta E_Q \approx 0.9$ mm/s and $\delta = 0.45$ mm/s, seems to reflect a situation where the excess electron is evenly delocalized among the three iron sites.[13] Configuration X has not been reported for other $[Fe_3S_4]^0$-containing proteins. In order to assess whether such an excited state becomes thermally accessible for the two synthetic clusters, we have studied their zero-field Mössbauer spectra at higher temperatures. The 200 K spectrum of **11**, shown in Figure 14E, exhibits the same 2:1 intensity pattern as the 4.2 K spectrum, showing that configuration X is not measurably populated at 200 K. The same result was obtained for **12**. The temperature dependencies of ΔE_Q and δ are listed in Table 5.

We have recorded Mössbauer spectra at 4.2 K in applied fields up to 8.0 T. Representative spectra are shown in Figures 15 and 16. Both complexes were observed to exhibit resolved magnetic hyperfine interaction in fields as low at 0.1 T, showing that the electronic spin fluctuates slowly on the time scale of Mössbauer spectroscopy. (The two lowest levels of the $S = 2$ system are separated by 0.3 cm^{-1}, and their spin expectation values are equal but have opposite signs. In the fast fluctuation

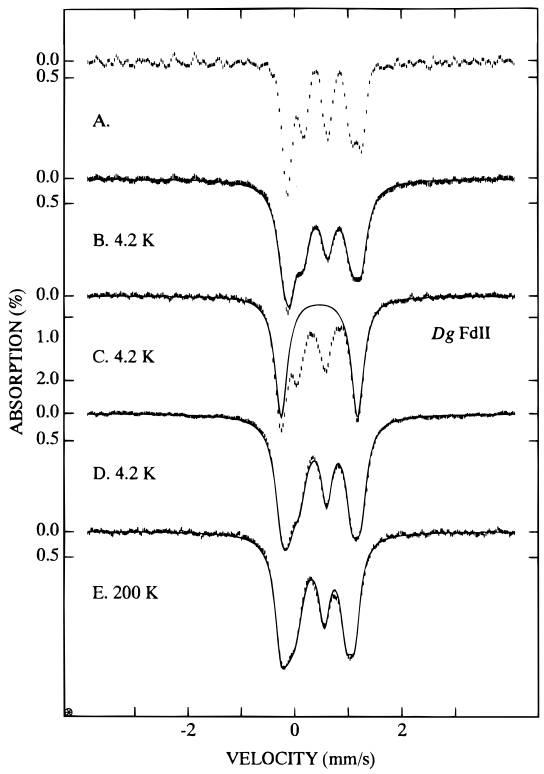

Figure 14. Mössbauer spectra of polycrystalline $(Et_4N)_3[Fe_3S_4(LS_3)]$ and $(Et_4N_3)[Fe_3Se_4(LS_3)]$ and of *Dg* Fd II recorded in zero applied magnetic field. (B) 4.2 K spectrum of $(Et_4N)_3[Fe_3Se_4(LS_3)]$. The spectrum in (A) was obtained from the data in (B) by removing the line width contribution of the ^{57}Co source. (C) 4.2 K spectrum of *Dg* Fd II; the solid line indicates the contribution of the delocalized Fe^{2+}-Fe^{3+} pair, and the innermost doublet belongs to the Fe^{3+} site. (D and E) Spectra of $(Et_4N)_3[Fe_3S_4(LS_3)]$. The solid lines in (B), (D), and (E) are least-squares fits to the data assuming three doublets. Typical line width parameters were 0.28−0.32 mm/s (full width at half maximum). The spectra of the synthetic clusters each contain ≈5% contaminant of a $[Fe_4Q_4]^{2+}$ species; this contribution ($\Delta E_Q = 1.2$ mm/s, $\delta = 0.45$ mm/s) has been subtracted from the raw data.

Table 5. Quadrupole Splittings and Isomer Shifts of $[Fe_3Q_4(LS_3)]^{3-}$ (mm/s)

		$[Fe_3S_4]^0$		$[Fe_3Se_4]^0$	
T (K)	site	ΔE_Q	δ	ΔE_Q	δ
4.2	P_1	1.48	0.49	1.45	0.52
	P_2	1.18	0.48	1.20	0.49
	Fe^{3+}	0.51	0.35	0.47	0.39
150	P_1	1.45	0.45	1.26	0.48
	P_2	1.11	0.44	0.94	0.46
	Fe^{3+}	0.49	0.32	0.45	0.39
200	P_1	1.38	0.43	1.24	0.46
	P_2	1.09	0.42	0.91	0.45
	Fe^{3+}	0.52	0.30	0.45	0.37

(69) Huynh, B. H.; Münck, E.; Orme-Johnson, W. H. *Biochim. Biophys. Acta* **1979**, *527*, 192.

(70) Analysis of the spectra of all data sets suggests that **11** and **12** contain a *ca*. 5% contaminant of $[Fe_4S_4]^{2+}$ and $[Fe_4Se_4]^{2+}$ species, respectively. Both the zero-field and high-field spectra indicate additional absorbance in the spectral range where (diamagnetic) $[Fe_4Q_4]^{2+}$ clusters typically absorb. For instance, a fit with free intensities to the spectrum of Figure 14B yields 31% and 69% for the intensities of site 1 and the sum of sites P2 and P3, respectively, rather than the expected 33.3% and 66.7%. While these differences could be attributed to different recoiless fractions of the sites, this interpretation would not explain the additional absorption in the "diamagnetic regions" of the high-field spectra.

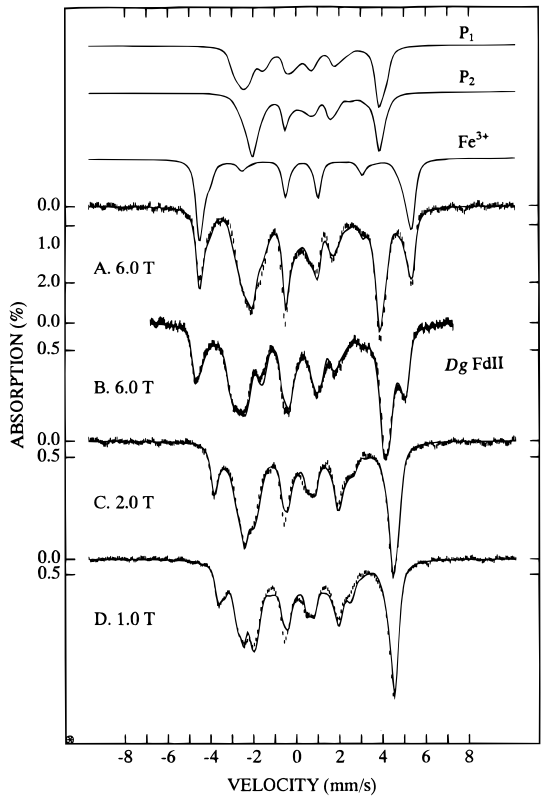

Figure 15. Mössbauer spectra of $(Et_4N)_3[Fe_3S_4(LS_3)]$ (A, C, D) recorded in magnetic fields applied parallel to the observed γ-radiation. For comparison, the 6.0 T spectrum of *Dg* Fd II is shown (B). Solid lines are theoretical spectra generated from eq 7 using the parameters in Table 6 for the case $\beta_A = 0$; P_1 and P_2 are components of the delocalized pair and Fe^{3+} is the ferric site.

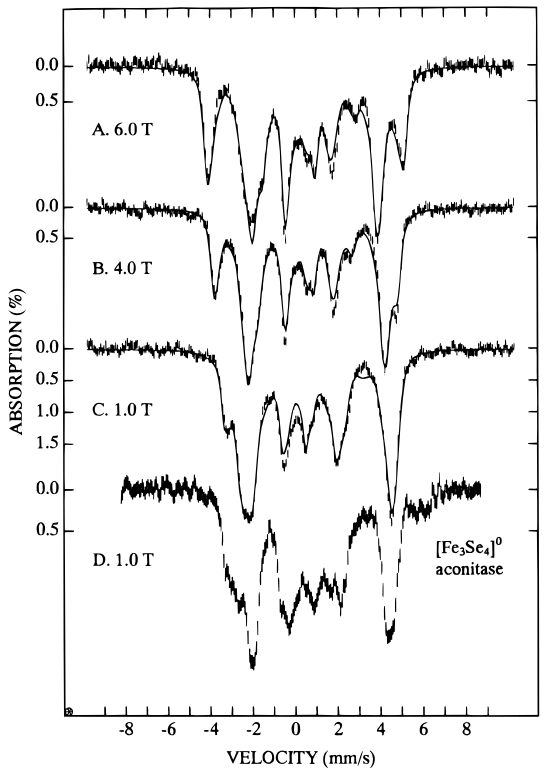

Figure 16. Mössbauer spectra of $(Et_4N)_3[Fe_3Se_4(LS_3)]$ (A, B, C) recorded in magnetic fields applied parallel to the observed γ-radiation. For comparison, the 1.0 T spectrum of the $[Fe_3Se_4]^0$ cluster in reconstituted aconitase[40] is shown (D). The solid lines are spectral simulations based on eq 7 using the parameters listed in Table 6.

limit only quadrupole doublets would be observed for $H = 0.1$ T.) It can be seen that the applied field spectra of both synthetic complexes are remarkably similar to those observed for protein-bound $[Fe_3S_4]^0$ (Figure 15B) and $[Fe_3Se_4]^0$ clusters (Figure 16D). We have analyzed the spectra of Figures 15 and 16 by using the same procedures as described previously.[13] The solid lines drawn through the spectra in these figures are theoretical curves generated from eq 7 with the parameters listed in Table 6.

All Mössbauer spectra of protein-bound Fe_3S_4 clusters reported thus far have been analyzed with the assumption that the **A** tensors of the three iron sites are collinear and that their principal axis frames coincide with the frame of the zero-field splitting tensor. Because the latter reflects a global property of the Fe_3S_4 cluster while the former describes the local sites, it is quite unlikely that this assumption is correct. However, the need to restrict the large number of unknowns (nearly 40 if all tensors of eq 7 have different principal axis frames) makes it impractical to allow the **A** tensors to occupy different principal axis frames. For applied fields <2.0 T, the Mössbauer spectra of each site are determined by the magnitude of $\mathbf{H}_{int} = -\langle \mathbf{S} \rangle \cdot \mathbf{A}/g_n\beta_n$ and the component of the electric field gradient tensor along H_{int}; only in strong applied fields are the spectra moderately sensitive to the orientations of the **A** tensors. Because the orientations of the **A** tensors are difficult to determine from the powder spectra, their principal components are somewhat soft. In order to explore this matter, we have fitted groups of high-field Mössbauer spectra by assuming a variety of fixed **A**-tensor orientations and letting a least-squares fitting program determine the best principal axis values of the **A** tensors. The parameters of one solution set for which the Euler angles for all three **A** tensors were set to $\alpha = \gamma = 0$ and $\beta = 30°$ are also listed in Table 6; here, α, β, and γ rotate the principal axis frame of each **A** tensor into the frame of the zero-field splitting tensor. The quality of the fit for $\beta = 30°$ is nearly the same as that of Figure 15. Interestingly, $A_{av} = (A_x + A_y + A_z)/3$ is quite independent of these rotations. This is fortunate, because this quantity is generally used for the evaluation of spin coupling models.

Figure 17 gives a comparison of the A_{av} values of **11** and **12** with those reported for protein-bound $[Fe_3S_4]^0$ clusters. It can be seen that the magnetic hyperfine interactions are nearly the same for all clusters, emphasizing once more the common electronic properties of all cuboidal Fe_3S_4 structures. As can be seen from the entries in Table 6, the zero-field splitting parameters are, within the experimental uncertainties, the same for all clusters. Congruence of the electronic properties is also expressed by the similarities in the quadrupole splittings and the isomer shifts. The only quantity outside the common range is the isomer shift of the Fe^{3+} site of the *D. gigas* hydrogenase cluster. The value $\delta = 0.39$ mm/s suggests, perhaps, some delocalization of d-electron density from the delocalized pair toward the Fe^{3+}; however, such delocalization is not obvious from inspection of the other quantities. (The unusually small value listed for A_x of this site, $A_x = 9.3$ MHz, is not outside the common range since this quantity has an uncertainty[68] of ± 7 MHz.)

The two lowest electronic levels of the $S = 2$ system (the $M_S = \pm 2$ states in the limit $E = 0$) of protein-bound $[Fe_3S_4]^0$ clusters have an energy separation $\Delta \approx 3D(E/D)^2$ that is comparable with the microwave quantum of X-band EPR. Thus, an integer-spin EPR signal can usually be observed that provides an independent measure of Δ (for details see ref 71). Figure 18 shows parallel mode EPR spectra (solid lines) of polycrystalline **11** and **12**. The observed resonances are very similar to those found for the protein-bound clusters.[71] The

(71) Münck, E.; Surerus, K. K.; Hendrich, M. P. *Methods Enzymol.* **1993**, *227,* 463.

Table 6. Zero-Field Splittings and Hyperfine Parameters of **11**, **12**, and Protein-Bound $[Fe_3S_4]^0$ Clusters

	D (cm^{-1})	E/D	site[a]	δ (mm/s)	ΔE_Q (mm/s)	η	β[b]	γ	A_x (MHz)	A_y (MHz)	A_z (MHz)	A_{av} (MHz)	ref
11	−2.5	0.22	P_1	0.49	1.5	0.9	30	17	−20.7	−17.5	−15.5	−17.9	this work
			P_2	0.49	1.2	−0.1	0		−13.8	−21.2	−15.9	−17.0	
			Fe^{3+}	0.35	0.5	3.3	10		15.5	19.2	17.3	17.3	
11	−2.5	0.22	P_1	0.49	1.5	1.1	22	30	−16.8	−22.7	−15.3	−18.3	this work
($\beta_A = 30°$)[c]			P_2	0.49	1.2	0	5	10	−13.6	−20.7	−16.7	−17.0	
			Fe^{3+}	0.35	0.5	3.7	45	10	16.7	17.1	17.7	17.2	
Dg Fd II	−2.5	0.23	P	0.46	1.47	0.4	20		−20.5	−20.5	−16.4	−19.1	13
			Fe^{3+}	0.32	−0.52	−2	16		13.7	15.8	17.3	15.6	
Pf Fd	−2.5	0.23	P	0.47	1.54	0.4	20	0	−17	−25.9	−16.5	−19.8	36
			Fe^{3+}	0.30	0.48	0.3	106	90	16.9	17.6	14.1	16.2	
Av Fd I	−2.5	0.23	P_1	0.47	1.41	0	19		−20	−22	−16.7	−19.6	67
			P_2	0.47	1.41	1	27		−19	−27	−16.7	−20.9	
			Fe^{3+}	0.30	−0.47	5	0		16	14	17.2	15.7	
aconitase	−2.5	0.25	P_1	0.49	1.46	1	15		−19.2	−19.2	−15.1	−17.8	40
			P_2	0.46	1.15	0	25		−19.2	−19.2	−15.9	−18.1	
			Fe^{3+}	0.31	0.56	0	50		17.3	17.3	16.5	17.0	
Cv H	−2.8	0.22	P_1	0.47	1.44	0.9	25		−22	−19	−16.7	−19.2	66
			P_2	0.47	1.44	0.6	10		−20	−25	−16.3	−20.4	
			Fe^{3+}	0.32	0.59	0.9	65		16	17	17.4	16.8	
Dg H	−2.0	0.20	P	0.47	1.67	1	25		−20.5	−17.8	−15.8	−18.0	68
			Fe^{3+}	0.39	0.38	−1	45		9.3	17.8	17.4	14.8	
12	−2.5	0.20	P_1	0.52	1.45	1.2	10		−11.0	−20.0	−16.0	−15.7	this work
			P_2	0.49	1.2	−0.16	2		−14.0	−22.0	−15.5	−17.2	
			Fe^{3+}	0.39	0.47	2.2	2		15.0	12.0	16.2	14.4	

[a] P_1 and P_2 are the sites of the valence-delocalized $Fe^{2+}Fe^{3+}$ pair. [b] α, β, and γ are the Euler angles that rotate the electric field gradient tensor into the principal axis frame of the zero-field splitting tensor. [c] For this fit the z-axes of the three **A**-tensors were rotated by $\beta_A = 30°$ relative to the z-axis of the zero-field splitting tensor.

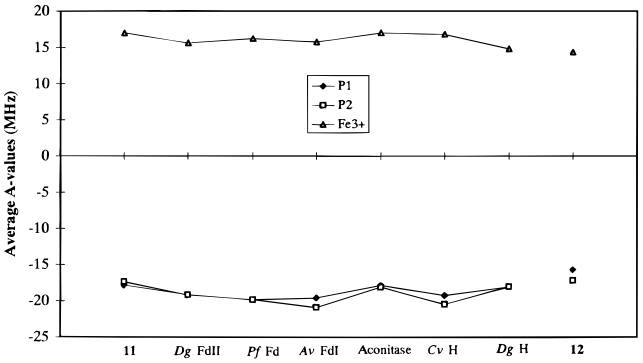

Figure 17. Average **A** values, $A_{av} = (A_x + A_y + A_z)/3$, for the Fe^{3+} site and the delocalized $Fe^{2+}Fe^{3+}$ pair of clusters **11** and **12** and protein-bound $[Fe_3S_4]^0$ clusters (H = hydrogenase).

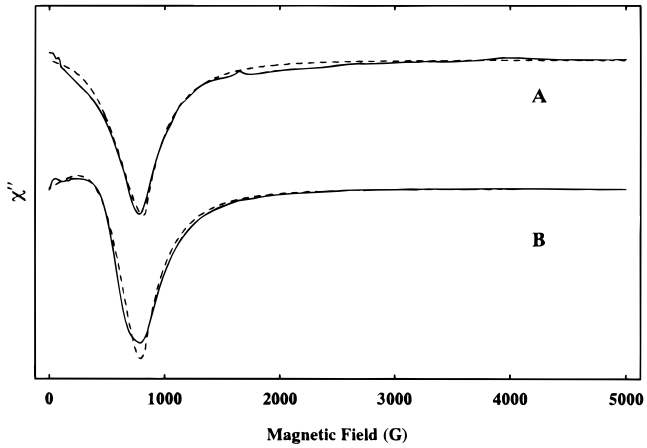

Figure 18. X-band EPR spectra of polycrystalline $(Et_4N)_3[Fe_3S_4(LS_3)]$ (A) and $(Et_4N)_3[Fe_3Se_4(LS_3)]$ (B) recorded in parallel mode. Dashed lines are theoretical spectra computed for $g_x = g_y = g_z = 2.0$ and the Δ and σ_Δ values quoted in the text. EPR conditions: $T = 9$ K; microwave frequency, 9.35 GHz; microwave power, 2 mW (upper spectrum) and 0.5 mV (lower spectrum); modulation amplitude, 2 mT. The compounds were suspended in Nujol.

dashed lines in Figure 18 are theoretical spectra computed for $\Delta \pm \sigma_\Delta = (0.28 \pm 0.12)$ cm^{-1} for **11** and $\Delta \pm \sigma_\Delta = (0.26 \pm 0.11)$ cm^{-1} for **12**; the width of the lines was modeled by assuming that the splitting of the EPR-active doublet, Δ, has a Gaussian distribution (width σ_Δ) about its mean value Δ. These values are in reasonable agreement with the Δ-values obtained by Mössbauer spectroscopy, namely $\Delta = 0.35$ cm^{-1} for **11** and $\Delta = 0.30$ cm^{-1} for **12**.

Summary. The following are the principal results and conclusions of this investigation, presented as replies to points (i)−(vi) raised at the outset.

(i) Clusters containing the $[Fe_3Q_4]^0$ cores (Q = S, Se) are readily prepared in yields of *ca.* 80−90% by iron atom abstraction from suitably ligated $[Fe_4Q_4]^{2+}$ clusters with 2−3 equiv of *N*-methylimidodiacetate. Unlike $[Fe_3S_4]^{1+}$ cluster formation in proteins and several earlier synthetic systems, no prior oxidation of the cubane precursor is required. No synthetic cluster containing a *discrete* cuboidal Fe_3Q_4 core has previously been isolated in substance.[72]

(ii) The preparation and stability of $[Fe_3Q_4]^0$ clusters are significantly promoted by use of the semi-rigid site-differentiating ligand LS_3.[76] The product species $[Fe_3Q_4(LS_3)]^{3-}$ are stable for days in anaerobic solution at ambient temperature. The cuboidal cluster $[Fe_3S_4(SEt)_3]^{3-}$, with conventional terminal ligands, can be formed and may be sufficiently stable to isolate, but is less stable to degradation to other clusters than is $[Fe_3S_4(LS_3)]^{3-}$. Clearly, a protein matrix is not *necessary* to

(72) Cuboidal Fe_3Q_4 is present as a fragment condensed into the higher-nuclearity molecular clusters $[Fe_6Q_9(SR)_2]^{4-}$ [73] and $[Na_2Fe_{18}S_{30}]^{8-}$, [74] and in an extended solid.[75]

(73) (a) Christou, G.; Sabat, M.; Ibers, J. A.; Holm, R. H. *Inorg. Chem.* **1982**, *21*, 3518. (b) Strasdeit, H.; Krebs, B.; Henkel, G. *Inorg. Chem.* **1984**, *23*, 1816; *Z. Naturforsch.* **1987**, *42B*, 565.

(74) (a) You, J.-F.; Snyder, B. S.; Papaefthymiou, G. C.; Holm, R. H. *J. Am. Chem. Soc.* **1990**, *112*, 1067. (a) You, J.-F.; Papaefthymiou, G. C.; Holm, R. H. *J. Am. Chem. Soc.* **1992**, *114*, 2697.

(75) Hong, H. Y.; Steinfink, H. *J. Solid State Chem.* **1972**, *5*, 93.

(76) Other ligands described as having the property of [1:3] iron site differentiation in Fe_4S_4 clusters may also suffice in this regard: (a) Whitener, M. A.; Peng, G.; Holm, R. H. *Inorg. Chem.* **1991**, *30*, 2411. (b) Evans, D. J.; Garcia, G.; Leigh, G. J.; Newton, M. S.; Santana, M. D. *J. Chem. Soc., Dalton Trans.* **1992**, 3229. (c) van Strijdonck, G. P. F.; van Haare, J. A. E. H.; van der Linden, J. G. M.; Steggerda, J. J.; Nolte, R. J. M. *Inorg. Chem.* **1994**, *33*, 999.

stabilize the Fe_3S_4 core, at least in the neutral oxidation state under ambient conditions.

(iii) The *ababab* ligand conformation and cuboidal core structure of $[Fe_3S_4(LS_3)]^{3-}$ have been proven by X-ray analysis. The $[Fe_3S_4]^0$ core is dimensionally closely related to the $[Fe_4S_4]^{2+}$ core of $[Fe_4S_4(LS_3)Cl]^{2-}$ and to the $[Fe_3S_4]^{1+,0}$ centers in *Av* Fd I and *Dg* Fd II. In turn, the latter are immediate structural derivatives of protein-bound $[Fe_4S_4]^{2+}$ clusters. Removal of an iron atom from a native or synthetic cubane core affords a cuboidal unit which is essentially congruent with the parent structure.

(iv) The clusters $[Fe_3Q_4(LS_3)]^{3-}$ in acetonitrile sustain a chemically reversible three-membered electron transfer series encompassing the oxidation states $[Fe_3S_4]^{1+,0,1-}$. The cationic and neutral states have been demonstrated in proteins. The protein-bound $[Fe_3S_4]^{1-}$ state has not been encountered unless stabilized by coordination of a metal ion in the vacant binding site. The highly negative $[Fe_3S_4]^{0,1-}$ potential (-1.72 V in acetonitrile) suggests that this and the all-ferrous $[Fe_3S_4]^{2-}$ state can only be achieved under physiological conditions by protonation or metal ion binding.

(v) The potential order of $E([Fe_4S_4(LS_3)L']^{2-,3-}) < E([Fe_3S_4(LS_3)]^{2-,3-})$ observed here and elsewhere[49,52] (L′ = monodentate anion) suggests that $E([Fe_4S_4]^{2+/1+}) \lesssim E([Fe_3S_4]^{1+/0})$ found for protein-bound clusters may be an inherent trend. However, with the synthetic cluster pair the difference in potential can be less than 100 mV, depending on L′ and solvent. The $[Fe_3S_4]^{1+/0}$ protein potentials are markedly variable, ranging from -70 mV (*Dg* hydrogenase[68]) to -460 mV (*Ac* Fd I[30c]) when reports of pH-dependent and pH-independent potentials are considered.

(vi) Comparison of isomer shifts, quadrupole splittings, zero-field splittings, and hyperfine parameters of synthetic clusters with those of protein-bound clusters leads to the inescapable conclusion that both have the same ground state and, for the most part, virtually indistinguishable electron distributions (Table 6). The electronic ground state of the cluster has cluster spin $S = 2$. This state arises from an interplay of two types of exchange interactions, namely double exchange between the two sites of the delocalized $Fe^{2+}Fe^{3+}$ (producing a dimer spin $S = {}^9/_2$) and antiferromagnetic exchange between the sites of the pair as well as between the Fe^{3+} site ($S = {}^5/_2$) and the sites of the pair. The importance of vibronic interactions for stabilizing the $S = 2$ ground state has been emphasized by Borshch et al.[17] Formation of the $S = 2$ ground state is an intrinsic property of the cluster and independent of protein structure. To an extent, this result is foreshadowed by proof of the same ground state in the spin-isolated clusters $[Fe_4S_4(LS_3)(t\text{BuNC})_3]^{1-}$ [50] and $[(OC)_3MoFe_3S_4(SEt)_3]^{3-}$ [51] whose $[Fe_3S_4]^0$ core fragments are, however, mildly perturbed versions of that in $[Fe_3S_4(LS_3)]^{3-}$.

We conclude that $[Fe_3S_4(LS_3)]^{3-}$ is an accurate synthetic analogue of the $[Fe_3S_4]^0$ state found in a considerable number of Fe−S proteins, and that $[Fe_3Se_4(LS_3)]^{3-}$ bears the same relation to selenide-reconstituted aconitase. Thus, these clusters provide the initial entry to the fundamental reaction chemistry of cuboidal Fe_3S_4. Observations thus far indicate that one reactivity aspect, incorporation of metal ions to afford heterometal MFe_3Q_4 cubane clusters as in point (vii), can be realized.

Acknowledgment. This research was supported at Harvard University by NIH Grant No. GM 28856 and at Carnegie Mellon University by NSF Grant No. MCB 9406224. We thank Dr. Cary Bauer for collection of X-ray data and Dr. J. R. Long for experimental assistance and valuable discussions.

Supporting Information Available: X-ray structural information, including tables of crystal and intensity collection data, positional and thermal parameters, interatomic distances and angles, and stereoviews (21 pages). This material is contained in many libraries on microfiche, immediately follows this article in the microfilm version of the journal, can be ordered from the ACS, and can be downloaded from the Internet; see any current masthead page for ordering information and Internet access instructions.

JA9537843